

PRUNE-THEN-QUANTIZE OR QUANTIZE-THEN-PRUNE? UNDERSTANDING THE IMPACT OF COMPRESSION ORDER IN JOINT MODEL COMPRESSION

006 **Anonymous authors**

007 Paper under double-blind review

ABSTRACT

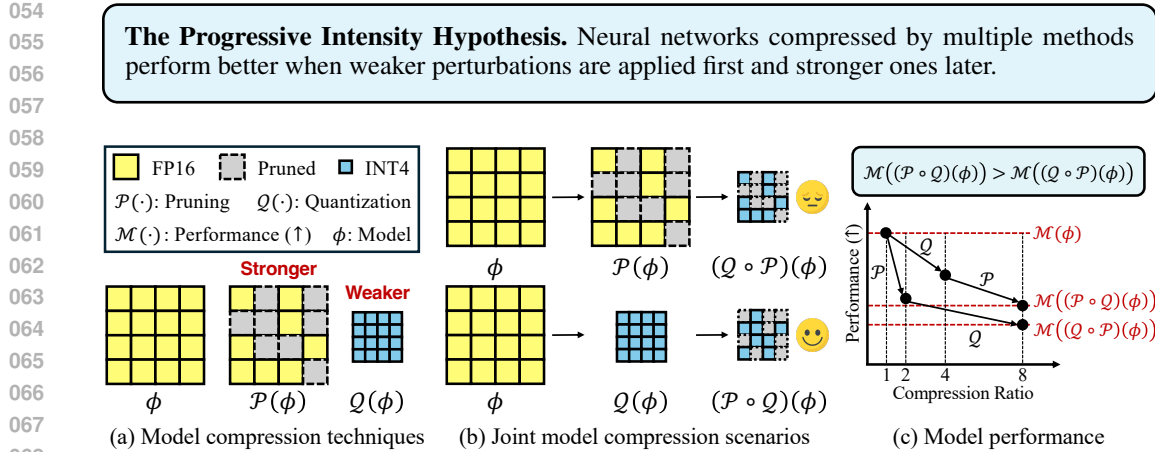
013 What happens when multiple compression methods are combined—does the or-
014 der in which they are applied matter? Joint model compression has emerged as
015 a powerful strategy to achieve higher efficiency by combining multiple methods
016 such as pruning and quantization. A central but underexplored factor in joint model
017 compression is the compression order, or the sequence of different methods within
018 the compression pipeline. Most prior studies have sidestepped the issue by assum-
019 ing orthogonality between techniques, while a few have examined them only in
020 highly constrained cases. Consequently, the broader role of compression order in
021 shaping model performance remains poorly understood. In this paper, we address
022 the overlooked problem of compression order and provide both theoretical and
023 empirical analysis. We formulate the problem of optimizing the compression order
024 and introduce the Progressive Intensity Hypothesis, which states that weaker pertur-
025 bations should precede stronger ones. We provide theoretical guarantees showing
026 that the relative benefit of one order increases with the underlying performance gap.
027 Extensive experiments on both language and vision models validate the hypothesis,
028 and further show its generality to broader setups such as multi-stage compression
029 and mixed-precision quantization.

1 INTRODUCTION

030 *When combining pruning and quantization, which order leads to better model performance?* Although
031 deep neural networks have achieved remarkable success across diverse domains, deploying them on
032 edge devices remains challenging due to limited computational resources. To bridge this gap, network
033 compression techniques (Deng et al., 2020; Liang et al., 2021; Zhu et al., 2024) have been proposed,
034 including pruning (Park et al., 2024; Song et al., 2024), quantization (Ashkboos et al., 2024b; Kim
035 et al., 2025), knowledge distillation (Tran et al., 2022; Xie et al., 2023), parameter sharing (Desai
036 & Shrivastava, 2024; Wang et al., 2025a) and low-rank approximation (Li et al., 2025; Wang et al.,
037 2025b). Recent studies highlight that combining these compression methods—known as *joint model*
038 *compression*—achieves better trade-offs between compression ratio and model performance than
039 applying them separately (Hawks et al., 2021; Wang et al., 2022; Shinde, 2024).

040 A critical yet underexplored issue in joint model compression is the *compression order*—the sequence
041 in which individual compression methods are applied to the target model. As most of these techniques
042 are not simultaneously applicable and should be executed sequentially (Wang et al., 2020; Kuzmin
043 et al., 2023), identifying an optimal order can yield a “free lunch” by improving performance without
044 any additional computation. Empirical findings (Huang et al., 2019; Hu et al., 2021; Qu et al.,
045 2025) show that the performance of the compressed model is sensitive to the compression order,
046 necessitating a deeper understanding of when and why certain orders work better.

047 However, the role of compression order has been largely overlooked by prior studies (Kurtic et al.,
048 2022; Xiao et al., 2023; Liu et al., 2023). Most existing studies implicitly assume that compression
049 order has no effect on the grounds of orthogonality, naïvely arguing that different techniques operate
050 independently without interfering with one another (Kim et al., 2021; Chitty-Venkata et al., 2023;
051 Song et al., 2024; Motetti et al., 2024). Only a few works have examined the problem, and most of
052 them merely offer empirical evidence confined to specific settings (Wang et al., 2020; Wu et al., 2023;
053



069
070
071
072
073
074
075
076
077
078
079
080
081
082
083
084
085
086
087
088
089
090
091
092
093
094
095
096
097
098
099
100
101
102
103
104
105
106
107

Figure 1: **The Progressive Intensity Hypothesis:** Given two compression techniques, we conjecture that compressed models perform better if the stronger method is applied after the weaker one. That said, the optimal order between pruning and quantization varies with their compression ratios.

Yu et al., 2023). One notable attempt (Harma et al., 2025) presents a theoretical framework, proving the non-orthogonality of pruning and quantization, concluding that pruning followed by quantization is always preferable. However, the scope of the work remains narrow and less practical, focusing only on magnitude-based pruning and max-scaled quantization (see Appendix D.5). To date, no study has systematically investigated the broader tendencies of compression order in general settings, neither empirically nor theoretically.

In this paper, we demonstrate that applying more aggressive compression algorithms at later stages yields superior performance. We first formulate the problem of *joint compression order optimization* (see Section 3.1 and Problem 1), and introduce *the Progressive Intensity Hypothesis*, which posits that ordering compression methods from weaker to stronger improves performance (see Hypothesis 1). Figure 1 offers a conceptual depiction of the proposed hypothesis. We validate our claim through both theoretical analysis and extensive experiments. Theoretically, we show that the advantage of the compression order grows monotonically with the performance gap between two methods under *disjoint sensitivity* (see Theorem 1 and Definition 5). In other cases, we define *interference* as an additional error from mutual interaction and investigate its influence (see Definition 6). Experimentally, we validate the hypothesis across both language and vision models, covering diverse model architectures, tasks, and compression scenarios (see Sections 5.2 and 5.3). Our analysis also considers how factors such as weight-update strategies and rotations affect the role of compression order (see Figures 4 and 5). Moreover, our results highlight that the hypothesis generalizes to broader paradigms, including multi-stage approaches and mixed-precision quantization (see Section 5.4).

Our contributions are summarized as follows:

- **Formulation.** We formally define the novel problem of optimizing the compression order in joint model compression (see Problem 1), and propose *the Progressive Intensity Hypothesis*, suggesting that stronger perturbations should be applied later to achieve better performance (see Hypothesis 1).
- **Theory.** We provide a theoretical analysis that quantifies the relationship between method interaction and order sensitivity. Specifically, we prove that the superiority of one ordering grows monotonically with the performance gap between the two methods (see Theorem 1).
- **Experiments.** Extensive and consistent experimental results across various domains, models, and tasks support our hypothesis (see Figures 3, 4, and 6). We further extend the problem to broader setups such as multi-stage compression and mixed-precision quantization (see Figures 7 and 10).

To the best of our knowledge, we are the first to both theoretically and experimentally analyze the impact of compression order in joint model compression under general and practical settings.

Reproducibility. All of our implementations are available at <https://anonymous.4open.science/r/PQQP/> and within the Supplementary Materials (Authors, 2026).

108

2 PRELIMINARIES AND RELATED WORKS

109
110 We briefly describe the preliminaries and related works on pruning, quantization, and joint model
111 compression. The notations used throughout this paper are formally defined in Appendix A.112
113 **Pruning and Quantization.** Compression¹ techniques aim to transform a pre-trained model ϕ as a
114 more efficient version ϕ' while minimizing performance degradation (Xu & McAuley, 2023; Dantas
115 et al., 2024; Liu et al., 2025a). This process inevitably introduces an error term $\delta(\cdot)$, representing
116 the deviation between outputs of ϕ' and ϕ , which typically increases with the compression ratio C .
117 We define the compression ratio C as the memory usage of ϕ divided by that of ϕ' . Among various
118 compression techniques $f(\phi; C)$, our work centers on two major forms: pruning and quantization.119
120 Pruning $\mathcal{P}(\cdot)$ directly discards less important components of a model to achieve the desired com-
121 pression ratio while retaining its most critical parts (Nova et al., 2023; Ashkboos et al., 2024a; Park
122 et al., 2024). Based on the level of granularity, pruning methods fall into three categories: structured
123 pruning (Song et al., 2024) removes entire structural elements such as layers, filters, or attention
124 heads, semi-structured pruning (Xu et al., 2024) enforces fixed sparsity patterns (e.g., 2:4 sparsity)
125 across tensors, and unstructured pruning (Frantar & Alistarh, 2023) prunes weights in a fully flexible
126 manner. In the case of structured pruning at the layer level, the induced error $\delta_{\mathcal{P}}(\mathbf{W}_i, \mathbf{X}_i)$ is $-\mathbf{W}_i \mathbf{X}_i$
127 when pruning is applied to layer l_i with weight \mathbf{W}_i and activation \mathbf{X}_i , and $\mathbf{0}$ otherwise. The model
128 achieves a compression ratio $C_{\mathcal{P}} = 1/(1-p)$ by pruning a fraction p of weights.129
130 Quantization $\mathcal{Q}(\cdot)$ reduces the bit precision used to represent weights and activations by encoding a
131 high-bit network into a lower-bit format (Gholami et al., 2022). Common quantization techniques
132 include uniform (Li et al., 2021), non-uniform (Zhao & Yuan, 2025), binary coding (Park et al., 2025),
133 and vector quantization (VQ) (Tseng et al., 2024). Although some techniques such as VQ focus only
134 on weight quantization without compressing activations, our main scope is on compressing both for
135 practical acceleration. A main challenge towards robust quantization is the activation outliers (Xiao
136 et al., 2023; Lee et al., 2024), but recent rotation-based methods (Lin et al., 2024; Liu et al., 2025b)
137 have largely overcome it. The layer-wise error by quantization $\mathcal{Q}(\cdot)$ for a layer l_i with weight \mathbf{W}_i
138 and activation \mathbf{X}_i is computed as $\delta_{\mathcal{Q}}(\mathbf{W}_i, \mathbf{X}_i) = \mathcal{Q}(\mathbf{W}_i)\mathcal{Q}(\mathbf{X}_i) - \mathbf{W}_i \mathbf{X}_i$, with a compression ratio
139 $C_{\mathcal{Q}} = B_{\text{orig}}/B_{\mathcal{Q}}$ depending on the original B_{orig} and target $B_{\mathcal{Q}}$ bit-widths.140
141 **Joint Model Compression.** Joint compression combines two or more compression methods, achiev-
142 ing higher compression ratios while minimizing performance loss (Wang et al., 2020; Wu et al.,
143 2023; Yu et al., 2023; Harma et al., 2025). These methods fall into two categories: co-designed and
144 post-hoc frameworks. Although the former offers the benefit of integration-aware design, they tend to
145 be method-specific and less adaptable to alternative configurations (Qu et al., 2025).146
147 In contrast, combining independently designed techniques allows for method-agnostic pipelines that
148 adapt easily to diverse architectures. Several pruning works (Kurtic et al., 2022; Xiao et al., 2023;
149 Song et al., 2024) empirically confirm that such combinations with quantization are both feasible
150 and beneficial. As independently designed techniques are applied one after another, the order of
151 compression plays a key role. However, the impact of compression order has not been adequately
152 examined in the current literature. We denote applying $f_1(\cdot)$ before $f_2(\cdot)$ as $f_1 \rightarrow f_2$ or $(f_2 \circ f_1)(\cdot)$.153

3 JOINT COMPRESSION ORDER OPTIMIZATION

154

3.1 PROBLEM DEFINITION

155
156 We are given a pre-trained model and multiple compression techniques, each associated with a specific
157 compression rate. The goal is to find the optimal order in which to sequentially apply these methods.
158 An order is considered optimal if it minimizes the degradation in model performance. We quantify
159 performance using a metric $\mathcal{M}(\cdot)$, where higher values indicate better outcomes (e.g., classification
160 accuracy or the negative of perplexity). We provide the formal definition as Problem 1.161 **Problem 1** (Joint Compression Order Optimization). *We have a pre-trained model ϕ , a set of
162 compression methods $\mathbb{F} = \{f_1(\cdot), f_2(\cdot), \dots, f_n(\cdot)\}$, and a performance metric $\mathcal{M}(\cdot)$. For a set $\Pi =$
163 $\{\pi : \mathbb{F} \rightarrow \mathbb{F} \mid \pi \text{ is bijective}\}$ of all permutations over \mathbb{F} , the goal is to find the optimal permutation
164 $\pi^* \in \Pi$ that maximizes the performance of the compressed model: $\pi^* = \arg \max_{\pi \in \Pi} \mathcal{M}(\pi(\phi))$.*165
166 ¹In the remainder of the paper, we use ‘compression’ to refer to ‘model compression’ for simplicity.

162
163

3.2 CHARACTERIZING COMPRESSION ATTRIBUTES

164
165
166

Two key attributes arise when characterizing compression in a general setting: granularity and intensity. Granularity refers to the smallest structural unit on which compression is applied, and intensity refers to how aggressively the method alters the model, measured by its impact on performance.

167
168
169
170
171
172
173
174

Granularity of Compression. Compression methods are not applied to the model as a whole, but rather operate locally on its individual components. We define compression granularity as the atomic level at which compression is performed. To formalize this notion, we begin by abstracting the model into a set of component types, such as layers, sublayers, or attention heads. We refer to these as *abstract types*, which define the structural units over which compression may act. For two abstract types t_1 and t_2 , we say t_1 is *larger* than t_2 if t_1 strictly contains t_2 as a structural unit. Among all types that are larger than both t_1 and t_2 , we define the *least upper type* $t_{\text{lut}}(t_1, t_2)$ as the smallest one. For a given model ϕ , let \mathcal{T}_ϕ denote the set of abstract types; this set depends on the model architecture.

175
176
177
178

Each compression method $f(\cdot)$ may be applicable only to a subset of abstract types. We denote this subset by $\mathcal{T}_f \subseteq \mathcal{T}_\phi$, representing the structural levels at which $f(\cdot)$ can operate. For instance, layer-wise pruning in large language models is applicable only to units coarser than layers. Then, the granularity of $f(\cdot)$ is the smallest unit $t_f \in \mathcal{T}_f$ on which $f(\cdot)$ is applicable, as defined in Definition 1.

179
180
181
182

Definition 1 (Compression Granularity). *For a model ϕ with a set \mathcal{T}_ϕ of abstract types and compression method $f(\cdot)$, the compression granularity $t_f := \arg \min_{t \in \mathcal{T}_f} |t|$, where $\mathcal{T}_f \subseteq \mathcal{T}_\phi$ denotes the set of abstract types on which $f(\cdot)$ operates, and $|t|$ denotes the structural size of type t .*

183
184
185
186

Intensity of Compression. Compression methods affect the model differently even at identical compression ratios, so comparing their intensities directly is challenging. To assess compression strength, we introduce three concepts grounded in performance degradation: performance gap $\mathcal{G}(f_1, f_2)$, compression equivalent ratio C_f^* , and compression order advantage $\mathcal{A}(f_1 \rightarrow f_2)$.

187
188
189
190

Performance differences between two methods $f_1(\cdot; C_1)$ and $f_2(\cdot; C_2)$, each applied at its respective compression ratios C_1 and C_2 , provide a direct measure of their relative intensity. We call this the *performance gap* $\mathcal{G}(\phi, \mathcal{M}; f_1(\cdot; C_1), f_2(\cdot; C_2))$, or simply $\mathcal{G}(f_1, f_2)$, as defined in Definition 2. If $\mathcal{G}(f_1, f_2) > 0$, we refer to $f_2(\cdot; C_2)$ as the stronger compression and $f_1(\cdot; C_1)$ as the weaker one.

191
192
193

Definition 2 (Performance Gap). *Given a model ϕ , a performance metric $\mathcal{M}(\cdot)$, and two compression methods $f_1(\cdot; C_1)$ and $f_2(\cdot; C_2)$, the performance gap between two methods $\mathcal{G}(\phi, \mathcal{M}; f_1(\cdot; C_1), f_2(\cdot; C_2)) := \mathcal{M}(f_1(\phi; C_1)) - \mathcal{M}(f_2(\phi; C_2))$.*

194
195
196
197
198
199
200
201
202
203
204
205

Although $\mathcal{G}(\cdot)$ offers a clear pairwise comparison, its values in metric units are difficult to interpret and may grow rapidly as the compression ratio increases. Alternatively, mapping methods onto a common scale allows for direct comparison at the level of compression ratios. While multiple choices exist for the baseline method, we select quantization as it exhibits the best performance across diverse models, thereby offering the widest range. Accordingly we define the Compression Equivalent Ratio (CER) $C^*(f_1(\cdot), \mathcal{Q}, C)$, or simply $C_{f_1}^*$, which expresses the effect of method $f_1(\cdot; C)$ at ratio C as an equivalent ratio of quantization $\mathcal{Q}(\cdot)$, as Definition 3. In other words, starting from a 16-bit model, a compression method $f(\phi; C)$ with $C_f^* = 2$ achieves the same performance as 8-bit quantization. Note that CER of quantization $\mathcal{Q}(\cdot)$ is naturally equal to its own compression ratio (i.e., $C_{\mathcal{Q}}^* = C_{\mathcal{Q}}$). We adopt a straightforward approach by computing CER through linear interpolation. For instance, $f(\cdot)$ achieving $\mathcal{M}(f; C) = 65\%$ accuracy maps to $C_f^* = 3$ when quantization $\mathcal{Q}(\cdot)$ yields $\mathcal{M}(\mathcal{Q}; C_{\mathcal{Q}} = 2) = 70\%$ and $\mathcal{M}(\mathcal{Q}; C_{\mathcal{Q}} = 4) = 60\%$ accuracy, respectively.

206
207
208
209

Definition 3 (Compression Equivalent Ratio). *Given a model ϕ , a performance metric $\mathcal{M}(\cdot)$, a compression method $f(\cdot)$, a quantization method $\mathcal{Q}(\cdot)$, and a compression ratio C , the compression equivalent ratio $C^*(f(\cdot), \mathcal{Q}, C) := C'$ such that $\mathcal{M}(\mathcal{Q}(\phi; C')) = \mathcal{M}(f(\phi; C))$.*

210
211
212
213

Until now our discussion is limited to single methods; but when multiple methods are applied, how should intensity be defined? Our scope centers on measuring how intensity changes by compression order. Accordingly, we capture the gain from applying $f_1(\cdot)$ before $f_2(\cdot)$ over the reverse as compression order advantage $\mathcal{A}(\phi, \mathcal{M}; f_1(\cdot) \rightarrow f_2(\cdot))$, or simply $\mathcal{A}(f_1 \rightarrow f_2)$, as Definition 4.

214
215

Definition 4 (Compression Order Advantage). *Given a model ϕ , a performance metric $\mathcal{M}(\cdot)$, and two compression methods $f_1(\cdot; C_1)$ and $f_2(\cdot; C_2)$, the compression order advantage $\mathcal{A}(\phi, \mathcal{M}; f_1(\cdot; C_1) \rightarrow f_2(\cdot; C_2)) := \mathcal{G}(f_1 \rightarrow f_2, f_2 \rightarrow f_1) = \mathcal{M}((f_2 \circ f_1)(\phi)) - \mathcal{M}((f_1 \circ f_2)(\phi))$.*

216 3.3 THE PROGRESSIVE INTENSITY HYPOTHESIS
217

218 Our goal is to uncover general patterns in how compression order affects the model performance
219 in joint compression scenarios. While prior works have focused primarily on isolated settings, we
220 seek to establish a broadly applicable principle. To this end, we propose *the Progressive Intensity*
221 *Hypothesis*, which posits that applying stronger compression methods at later stages generally yields
222 better performance. We formalize this hypothesis for a pair of methods in Hypothesis 1, which serves
223 as the main focus of our analysis; its extension to multiple methods is presented in Appendix B.3.

224 **Hypothesis 1** (The Progressive Intensity Hypothesis). *Let $f_1(\cdot; C_1)$ and $f_2(\cdot; C_2)$ be two compression
225 methods applied to a model ϕ . Then, the compression order advantage $\mathcal{A}(f_1 \rightarrow f_2)$ grows
226 monotonically with the performance gap $\mathcal{G}(f_1, f_2)$, or equivalently with the CER difference $C_{f_2}^* - C_{f_1}^*$.*

227 As an example, if methods $f_1(\cdot)$ and $f_2(\cdot)$ yields $\mathcal{M}(f_1; C_1) = 75\%$ and $\mathcal{M}(f_2; C_2) = 70\%$ accuracy,
228 respectively (i.e., $\mathcal{G}(\mathcal{P}, \mathcal{Q}) = 5\%$), the compression order advantage $\mathcal{A}(f_1 \rightarrow f_2)$ is mild; replacing
229 C_2 into C'_2 at $\mathcal{M}(f_2; C'_2) = 60\%$ accuracy (i.e., $\mathcal{G}(f_1, f_2) = 15\%$) results in a larger advantage.
230

231 4 THEORETICAL ANALYSIS
232

233 We theoretically analyze how compression order affects model performance. We introduce disjoint
234 selectivity to isolate order-dependent units, and prove in Theorem 1 that only these units determine
235 the performance gap. We then show in Theorem 2 that Hypothesis 1 holds due to the reduction of
236 order-dependent units. We extend to non-disjoint cases in which interference occurs. Consistent with
237 earlier works (Sun et al., 2024; Harma et al., 2025), we investigate each unit, relying on Assumption 1.

238 **Assumption 1.** *Given a model ϕ with a set \mathbb{L} of layers, performance metric $\mathcal{M}(\cdot)$, a compression
239 method $f(\cdot)$, and the layer-wise reconstruction loss $\delta_f(l_i)$, assume the followings:*

240 • **Layer-wise independence.** *The reconstruction error at one layer does not affect the reconstruction
241 error at another: $\forall l_i, l_j \in \mathbb{L}, i \neq j : \partial \delta_f(l_i) / \partial \delta_f(l_j) = 0$.*
242 • **Error-performance trade-off.** *Model performance is inversely related to total reconstruction error:
243 $\exists \beta > 0, \mathcal{M}(\phi) - \mathcal{M}(f(\phi)) = \beta \cdot \sum_{l_i \in \mathbb{L}} \|\delta_f(l_i)\|_F^2$.*

245 **Disjoint Selectivity.** Sequential application of two compression methods leads to two distinct scenarios: either there exist units altered by both methods, or all units are exclusively assigned to one. We
246 define the latter scenario as the case where *disjoint selectivity* holds, as in Definition 5. This means
247 that while the assignment may vary with order, each unit is ultimately handled by only one method.

248 **Definition 5** (Disjoint Selectivity). *Given a model ϕ , two compression methods $f_1(\cdot)$ and $f_2(\cdot)$ with
249 respective granularities t_{f_1} and t_{f_2} , disjoint selectivity holds if $\forall u_i \in \mathbb{U}(\phi; t_{lu}(t_{f_1}, t_{f_2}))$, $\forall \pi \in$
250 $\{f_1 \circ f_2, f_2 \circ f_1\}$, $\mathbb{D}_{u_i}^{f_1}(\pi) + \mathbb{D}_{u_i}^{f_2}(\pi) = 1$, where $\mathbb{U}(\phi; t)$ is the set of all units of model ϕ at granularity
251 t , and $\mathbb{D}_u^f(\pi)$ denotes whether $f(\cdot)$ modifies unit u under the order π (i.e., 1 if modified, 0 otherwise).*

252 Under disjoint selectivity, the compression order advantage $\mathcal{A}(f_1 \rightarrow f_2)$ is proportional to the
253 cumulative sum of error difference $g(\cdot)$ across units assigned differently depending on the order as
254 formulated in Theorem 1. The underlying intuition is that the performance gap rises solely from units
255 whose assignment varies with the order; for others, the error remains invariant and thus cancels out.
256 To illustrate, consider units u_1, u_2 , and u_3 and compression methods $f_1(\cdot)$ and $f_2(\cdot)$. If u_1 is always
257 handled by $f_1(\cdot)$ regardless of the order, while u_2 and u_3 are assigned differently depending on the
258 order, then the advantage $\mathcal{A}(f_1 \rightarrow f_2)$ is proportional to error difference of units u_2 and u_3 .

259 **Theorem 1** (Compression Order Advantage under Disjoint Selectivity). *Suppose we compress a
260 model ϕ with two compression methods $f_1(\cdot)$ and $f_2(\cdot)$ with respective granularities t_{f_1} and t_{f_2} ,
261 where disjoint selectivity holds. Then, under Assumption 1, the compression order advantage*

$$262 \mathcal{A}(f_1 \rightarrow f_2) = \mathcal{M}((f_2 \circ f_1)(\phi)) - \mathcal{M}((f_1 \circ f_2)(\phi)) = \beta \cdot \left(\sum_{u_i \in \mathbb{G}_2} g(u_i) - \sum_{u_i \in \mathbb{G}_1} g(u_i) \right),$$

263 where $g(u_i) = \|\delta_{f_1}(u_i)\|_F^2 - \|\delta_{f_2}(u_i)\|_F^2$ for error $\delta_f(u_i)$ on unit u_i by $f(\cdot)$, and groups $\mathbb{G}_1 =$
264 $\{u \mid \mathbb{D}_u^{f_1}(f_2 \circ f_1) = 1, \mathbb{D}_u^{f_1}(f_1 \circ f_2) = 0\}$ and $\mathbb{G}_2 = \{u \mid \mathbb{D}_u^{f_1}(f_2 \circ f_1) = 0, \mathbb{D}_u^{f_1}(f_1 \circ f_2) = 1\}$.

265 *Proof.* Refer to Appendix B.1. □

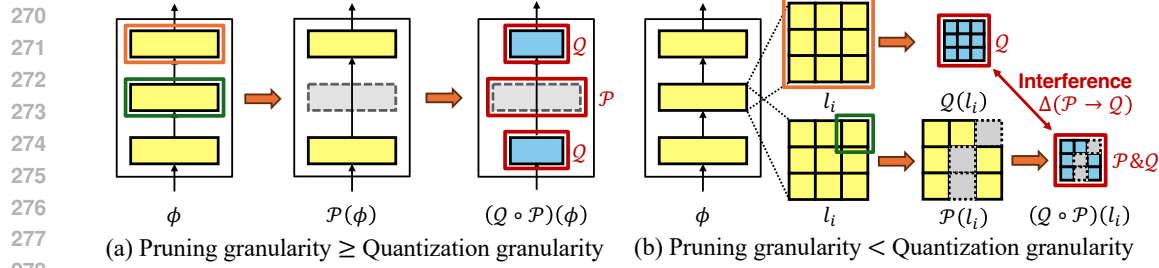


Figure 2: A case study of pruning $\mathcal{P}(\cdot)$ and quantization $\mathcal{Q}(\cdot)$ on model ϕ . (a) if pruning granularity (green) is coarser or equal to quantization granularity (orange), disjoint selectivity holds. (b) Otherwise, partial removal of quantization units by pruning introduces extra error, termed *interference* Δ .

Monotonicity. Under disjoint selectivity, we show that Hypothesis 1 holds when the two compression methods are *well-designed*—that is, minimally disruptive to the model. We examine this through a case study on pruning and quantization. We assume a favorable scenario where pruning is configured to induce minimal degradation, and quantization introduces symmetric, zero-mean errors centered at the original values. These assumptions are formalized in Assumption 2.

Assumption 2. *Given a model ϕ with a set \mathbb{L} of layers and performance metric $\mathcal{M}(\cdot)$, assume that:*

- **Well-designed pruning $\mathcal{P}(\cdot)$.** *The pruning method is chosen from the set of pruning strategies that aim to preserve the model performance: $\mathcal{P}(\cdot) \in \mathbb{P}(\mathcal{C}_P)$ where $\mathbb{P}(\mathcal{C}_P) = \{\mathcal{P}_i(\cdot) | C(\mathcal{P}_i(\phi)) = C_P, \mathcal{M}(\phi) - \mathcal{M}(\mathcal{P}_i(\phi)) \leq \delta\}$ denotes the set of pruning strategies that satisfy the target ratio C_P while keeping performance degradation within a small budget δ .*
- **Well-designed quantization $\mathcal{Q}(\cdot)$.** *For all layers, quantized outputs follow a symmetric distribution around the original values: $\forall l_i \in \mathbb{L}, \mathcal{Q}(\mathbf{W}_i)\mathcal{Q}(\mathbf{X}_i) \sim \mathcal{N}(\mathbf{W}_i\mathbf{X}_i, \sigma_Q^2 \mathbf{I})$, where $\mathcal{N}(\cdot)$ is the Gaussian distribution. The quantization error is negligible (i.e., $\mathcal{Q}(\mathbf{W}_i)\mathcal{Q}(\mathbf{X}_i) - \mathbf{W}_i\mathbf{X}_i \ll \mathbf{W}_i\mathbf{X}_i$).*

Theorem 2 states that when disjoint selectivity holds and the compression methods are well-designed, $\mathcal{A}(\mathcal{Q} \rightarrow \mathcal{P})$ increases monotonically with CER difference² $C_P^* - C_Q$ for fixed C_P . Note that as C_Q increases, compressed performance degrades and both CER difference $C_P^* - C_Q$ and performance gap $\mathcal{G}(\mathcal{Q}, \mathcal{P})$ increase monotonically. We show that $\mathcal{A}(\mathcal{Q} \rightarrow \mathcal{P})$ increases in this setting because the gap depends solely on order-dependent units under Theorem 1 and their reduction yields monotonic growth. We discuss the impact of C_P in Appendix D.6.

Theorem 2 (Monotonicity). *Suppose we compress a model ϕ with pruning $\mathcal{P}(\cdot)$ and quantization $\mathcal{Q}(\cdot)$, where disjoint selectivity holds. Then, under Assumptions 1 and 2, given performance metric $\mathcal{M}(\cdot)$ and two pairs of compression ratios $(C_{\mathcal{P}_1}, C_{\mathcal{Q}_1})$ and $(C_{\mathcal{P}_2}, C_{\mathcal{Q}_2})$, if CER difference increases*

$$C_{\mathcal{P}_1}^* - C_{\mathcal{Q}_1} > C_{\mathcal{P}_2}^* - C_{\mathcal{Q}_2},$$

then, the compression order advantage increases monotonically:

$$\mathcal{A}(\phi, \mathcal{M}; \mathcal{Q}(\cdot; C_{\mathcal{Q}_1}) \rightarrow \mathcal{P}(\cdot; C_{\mathcal{P}_1})) \geq \mathcal{A}(\phi, \mathcal{M}; \mathcal{Q}(\cdot; C_{\mathcal{Q}_2}) \rightarrow \mathcal{P}(\cdot; C_{\mathcal{P}_1})).$$

Proof. Refer to Appendix B.2. □

Granularity and Interference. Disjoint selectivity does not always hold in practical joint compression settings for pruning and quantization. As pruning operates by fully discarding or keeping each unit, it always satisfies disjoint selectivity. In contrast, quantization satisfies this condition only when its granularity is finer than or equal to that of pruning. Figure 2 illustrates this: (a) if $t_{\mathcal{P}} \geq t_{\mathcal{Q}}$, disjoint selectivity is preserved as pruning removes entire quantization units. However, (b) if $t_{\mathcal{P}} < t_{\mathcal{Q}}$, pruning may partially eliminate a quantization unit, introducing regions where both methods interfere.

In general joint compression of two methods $f_1(\cdot)$ and $f_2(\cdot)$, this violation of disjoint selectivity introduces additional error, which we define as *interference* $\Delta(\phi; f_1 \rightarrow f_2)$, or simply $\Delta(f_1 \rightarrow f_2)$ in Definition 6. Intuitively, interference quantifies how one method disturbs the behavior of the other.

Definition 6 (Interference). *Given a model ϕ and two methods $f_1(\cdot)$ and $f_2(\cdot)$, the interference*

$$\Delta(\phi; f_1 \rightarrow f_2) := \sum_{u \in \mathbb{X}} (\delta_{f_2 \circ f_1}(u) - \delta_{f_2}(u)), \text{ where } \mathbb{X} = \mathbb{U}(\phi; t_{f_2}) \cap \{u \mid \mathbb{D}_u^{f_2}(f_2 \circ f_1) = 1\},$$

²By definition, quantization serves as the baseline scale, so its CER equals its own compression ratio (i.e., $C_Q^* = C_Q$). Therefore, $C_P^* - C_Q$ represents the CER difference between pruning and quantization.

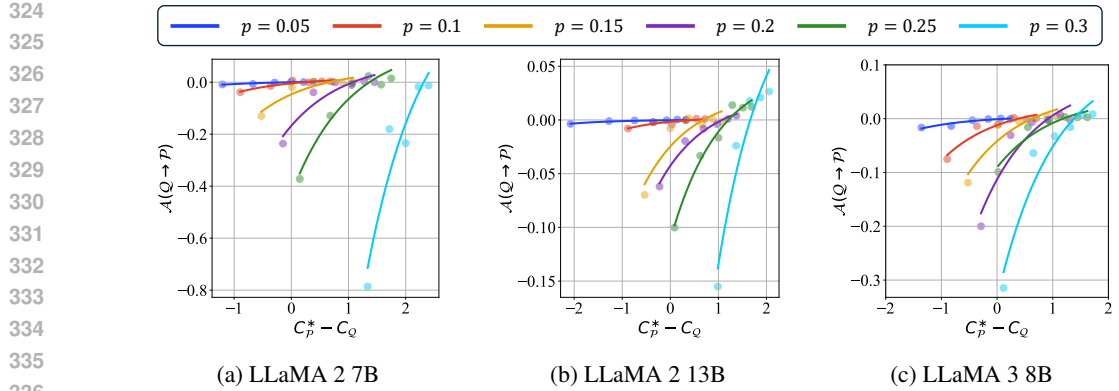


Figure 3: Across diverse language models, the compression order advantage $\mathcal{A}(Q \rightarrow P)$ increases monotonically with the CER difference $C_P^* - C_Q$. See Section 5.2 for details.

set $\mathbb{U}(\phi; t)$ contains all units of model ϕ at type t , $\mathbb{D}_u^f(\pi)$ indicates whether unit u is modified by $f(\cdot)$ under order π (1 if modified, 0 otherwise), and $\delta_{f(\cdot)}(u)$ denotes the error on u after applying $f(\cdot)$.

Interference may or may not occur, depending on its applied techniques. A notable example is mixed-precision quantization, where treating each bit-width quantization as a distinct method satisfies disjoint selectivity, thereby avoiding interference. In our primary focus of pruning and quantization, interference arises solely from pruning, meaning that as the pruning ratio p increases, a larger portion of each unit is removed, leading to greater interference. Consequently, while exact outcomes may vary, $\mathcal{A}(f_1 \rightarrow f_2)$ remains a monotonic function of $C_P^* - C_Q$, even under interference. In conclusion, Hypothesis 1 holds under both disjoint and interfering scenarios, highlighting its general validity.

5 EXPERIMENTAL FINDINGS

We empirically validate our hypothesis in joint compression scenarios, starting with pruning and quantization on language and vision models. We then extend to general pipelines beyond them.

5.1 EXPERIMENTAL SETUP

We briefly introduce the experimental setup. Further setups are detailed in Appendix C.

Setup. For language models, we focus on decoder-only LLMs, mainly LLaMA (Touvron et al., 2023) and ViT models. The main metric is the negative of perplexity on WikiText-2 (Merity et al., 2017) dataset; results on commonsense reasoning tasks appear in Appendix D.3. For vision models, we evaluate the classification accuracy of ResNet-18 (He et al., 2016) (CNNs) and DeiT-Base (Touvron et al., 2021) (ViTs) models on ImageNet (Deng et al., 2009) dataset.

Baselines. We evaluate three pruning (SparseGPT (Frantar & Alistarh, 2023), Wanda (Sun et al., 2024), SLEB (Song et al., 2024)) and four weight-activation quantization methods (RTN (Gupta et al., 2015), OPTQ (Frantar et al., 2023), QuaRot (Ashkboos et al., 2024b), QuaRot + OPTQ) for language models. For vision models, we apply PRACTISE (Wang & Wu, 2023) and N2UQ (Liu et al., 2022) for CNNs, and adopt SAViT (Chuanyang et al., 2022) and RepQ-ViT (Li et al., 2023) for ViTs.

5.2 ANALYSIS ON LANGUAGE MODELS

We verify whether Hypothesis 1 holds for language models. Then, we analyze the effect of weight updates and rotations in quantization, and investigate the impact of pruning granularity on interference.

Compression Order Advantage by CER Differences. We analyze how the compression order advantage $\mathcal{A}(Q \rightarrow P)$ varies with CERs for SparseGPT ($P(\cdot)$) and QuaRot ($Q(\cdot)$) across three models: LLaMA 2 7B, 13B, and LLaMA 3 8B. Figure 3 confirms that both terms increase monotonically for all three models. **Each point in the figure corresponds to a compression ratio pair (C_P, C_Q) , defined by pruning ratio $p \in [0.05, 0.1, 0.15, 0.2, 0.25, 0.3]$ and quantization bit-width $B_Q \in [4, 5, 6, 7, 8]$.** We fit an exponential curve per pruning ratio p , reflecting the underlying trend. In this setting, the

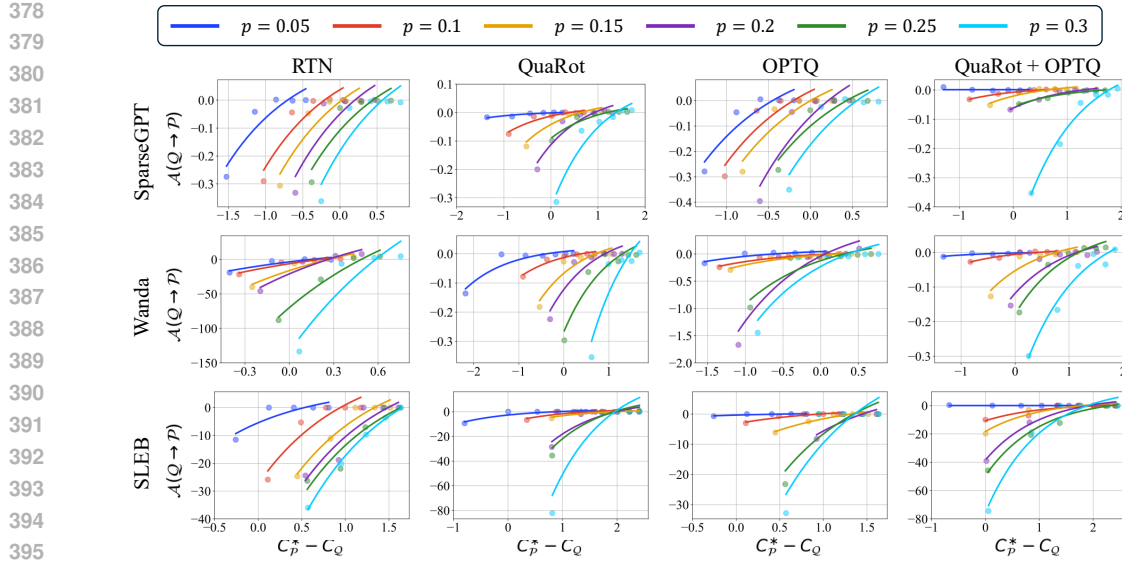


Figure 4: Compression order advantage $\mathcal{A}(Q \rightarrow P)$ against CER difference $C_P^* - C_Q$ for three pruning $\mathcal{P}(\cdot)$ and four quantization $Q(\cdot)$ methods on a LLaMA 3 8B model. Our hypothesis consistently holds for language models regardless of pruning granularity, rotation, and weight updates.

x-axis $C_P^* - C_Q$ captures the difference between the intrinsic intensities of pruning and quantization, with both C_P^* and C_Q calibrated on the original model ϕ . These values are not recalculated within joint pipelines; instead, they remain fixed reference scales, and the observed order advantage (y-axis) reflects the interaction between the two methods. Such consistent monotonic trends supports the validity of Hypothesis 1 across diverse language model architectures and scales; see Appendices D.1 and D.2 for results on encoder-based and other decoder-only models, respectively.

Finding 1. The Progressive Intensity Hypothesis holds across diverse language models of varying scales and architectures, showing that stronger compression should be applied later.

Weight Updates and Rotation-based Transformations. We investigate the hypothesis under practical techniques such as weight-updates and rotations. Figure 4 shows that Hypothesis 1 consistently holds across diverse combinations of methods. Our framework is agnostic to the type of compression methods; weight updates and rotations reduce quantization error, thereby increasing C_P^* .

Finding 2. The hypothesis generalizes beyond specific design choices of pruning and quantization, remaining robust under weight-update and rotation methods.

An intriguing phenomenon arises in pruning rotation-based methods: without quantization, pruning leads to a drastic performance drop compared to no rotation. Figure 5 illustrates the perplexity changes of a LLaMA 3 8B model pruned by SparseGPT, depending on QuaRot rotation. Increasing the pruning ratio amplifies the discrepancy between rotated and non-rotated settings, as pruning is applied without accounting for rotation. **This effect emerges because rotation may introduce two types of errors: *matrix-wise errors* from residual components and *instance-wise errors* from altered pruning decisions.** We further discuss the details in Appendix D.4 and Table 4. As rotation may intensify pruning, it is essential to design pruning approaches compatible with rotation-based quantization, the emerging *de facto* standard.

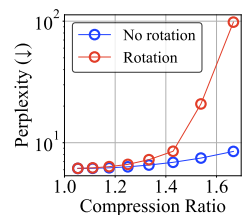
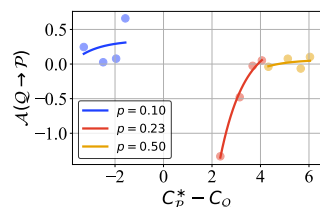
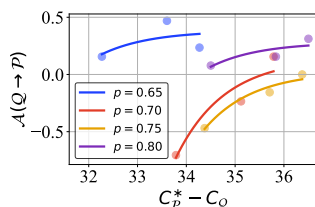


Figure 5: Rotation impact on pruning. See Section 5.2 for details.

Finding 3. Rotation alone amplifies pruning effects, underscoring the necessity of designing rotation-aware pruning methods.



(a) ResNet-18 (CNN)



(b) DeiT-Base (ViTs)

Figure 6: The Progressive Intensity Hypothesis holds across diverse vision models. See Section 5.3 for details.

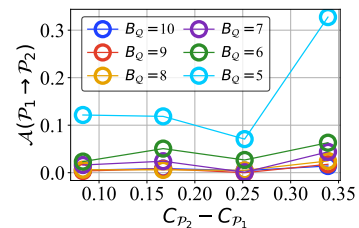


Figure 7: Multi-stage compression results on a LLaMA 3 8B model.

Table 1: $\mathcal{A}(\mathcal{Q} \rightarrow \mathcal{P})$ by quantization ratio C_Q .

C_Q (B_Q)	SparseGPT	SLEB
1.78 (9)	0.002	0
2.00 (8)	0.001	0
2.28 (7)	-0.003	0
2.68 (6)	-0.013	0
3.20 (5)	-0.017	-0.057
4.00 (4)	-49.899	-9.379

Pruning Granularity and Interference. We verify the presence of interference by comparing results across different pruning granularities. Table 1 reports $\mathcal{A}(\mathcal{Q} \rightarrow \mathcal{P})$ across different quantization bit-width B_Q when applying two 5% pruning methods with QuaRot. For SLEB, which applies structured pruning at sublayer level, there exists a regime where no layers differ in their pruning status across orders, leading to an exact $\mathcal{A}(\mathcal{Q} \rightarrow \mathcal{P})$ of zero (i.e., no interference). By contrast, SparseGPT, as an unstructured pruning method, exhibits interference in low C_Q ranges. Notably, empirical results suggest that interference also exhibits a monotonic trend regarding C_Q .

Finding 4. Pruning granularity determines interference: structured pruning shows no interference in early regimes, while unstructured pruning exhibits monotonic interference.

5.3 ANALYSIS ON VISION MODELS

We verify whether Hypothesis 1 holds for vision models, focusing on CNNs and ViTs.

CNN and ViT Models. In Figure 6, we analyze the behavior of ResNet-18 and DeiT-Base models under PRACTISE ($\mathcal{P}(\cdot)$) and N2UQ ($\mathcal{Q}(\cdot)$), and SAViT ($\mathcal{P}(\cdot)$) and RepQ-ViT ($\mathcal{Q}(\cdot)$) methods, respectively. The results confirm that both $\mathcal{A}(\mathcal{Q} \rightarrow \mathcal{P})$ and $C_P^* - C_Q$ increase monotonically for both models, regardless of the pruning or quantization configurations. Notably, the compression order advantage is substantially larger than that observed in language models, where it was often marginally positive. This is because vision models experience less performance degradation under higher compression rates C_P of pruning, thereby maintaining robust accuracy in the regime where the quantization-first advantage $\mathcal{A}(\mathcal{Q} \rightarrow \mathcal{P}) > 0$ (i.e., where C_P is high).

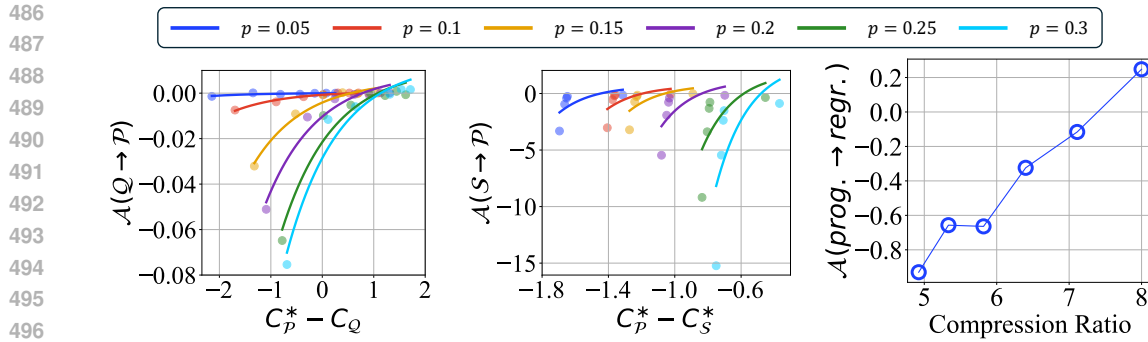
Finding 5. Vision models consistently satisfy the Progressive Intensity Hypothesis regardless of architecture and applied compression techniques, showing stronger quantize-then-prune gains $\mathcal{A}(\mathcal{Q} \rightarrow \mathcal{P})$ since pruning degrades them much less than in language models.

5.4 BEYOND PRUNING AND QUANTIZATION: TOWARD GENERAL PIPELINES

We extend the Progressive Intensity Hypothesis to general compression pipelines. These results align with the n -method ordering formulation in Appendix B.3.

Multi-stage Compression. Pruning is generally performed in multiple stages to mitigate performance degradation. In Figure 7, we investigate the impact of compression order by alternately applying SparseGPT ($\mathcal{P}(\cdot)$) and QuaRot ($\mathcal{Q}(\cdot)$) to the LLaMA 3 8B model where the sum of pruning ratios $p_1 + p_2 = 0.3$ (e.g., $\mathcal{P}(\cdot; C_{P_1}) \rightarrow \mathcal{Q}(\cdot) \rightarrow \mathcal{P}(\cdot; C_{P_2})$). Our results consistently demonstrate positive advantages, indicating that stronger pruning placed later improves performance under fixed quantization, confirming that our hypothesis holds not only for two stages but also for multiple ones.

Finding 6. Beyond pairwise orders, the hypothesis holds in practical multi-stage compression, indicating that scheduling stronger compression later in the sequence yields higher accuracy.

Figure 8: Joint compression re-
sults with LoRA adapters.Figure 9: Performance under
pruning and parameter sharing.Figure 10: The impact of com-
pression order in MPQ.

Parameter Efficient Fine-tuning. Parameter Efficient Fine-Tuning (PEFT), which introduces lightweight low-rank adapters to mitigate compression-induced performance degradation, has recently become a widely adopted practical approach. We investigate whether the proposed principle remains valid in scenarios where PEFT is applied alongside pruning and quantization. Figure 8 confirms that the same pattern holds for LLaMA 3 8B when combined with SparseGPT ($\mathcal{P}(\cdot)$), RTN ($\mathcal{Q}(\cdot)$), and LoRA (Hu et al., 2022) (PEFT). Applying LoRA after quantization produced a similar corrective effect to rotation, effectively compensating quantization-induced performance loss. Overall, the progressive intensity hypothesis remains robust under practical training pipelines that include PEFT.

Finding 7. PEFT preserves the hypothesis that stronger compression should be applied later, as post-quantization LoRA effectively restores accuracy and maintains the expected ordering.

Parameter Sharing. Beyond pruning and quantization, parameter sharing $\mathcal{S}(\cdot)$ is an independent compression technique that ties multiple layers into a unified set of weight parameters. We conduct joint compression experiments with pruning and parameter sharing to assess whether the principle generalizes beyond the pruning–quantization setting. In Figure 9, results on LLaMA 2 7B model with Basis Sharing (Wang et al., 2025a) ($\mathcal{S}(\cdot)$) and magnitude-based pruning (Han et al., 2015) ($\mathcal{P}(\cdot)$) confirm that the same ordering effect emerges as well.

Finding 8. Joint compression with parameter sharing also follows the hypothesis: placing the stronger operation later yields better performance.

Mixed-precision Quantization. As previously discussed, Mixed Precision Quantization (MPQ) can be formulated as a joint compression problem where each bit-width allocation acts as a separate compression method, satisfying disjoint selectivity. Figure 10 illustrates the effect of compression order in MPQ, where we sequentially allocate bit-widths using HAWQ-V2 on ResNet-18. As the total compression ratio increases, progressive allocation (prog.; 8 → 2 bits) increasingly outperforms regressive allocation (regr.; 2 → 8 bits), in terms of $\mathcal{A}(\text{prog.} \rightarrow \text{regr.})$. As the overall compression ratio increases, lower-bit quantization becomes stronger, which supports the hypothesis in MPQ.

Finding 9. The Progressive Intensity Hypothesis also holds in MPQ, with progressive bit allocation outperforming regressive allocation since lower-bit quantization acts as stronger compression.

6 CONCLUSION

We address the under-explored problem of joint compression order optimization and provide both theoretical and experimental evidences. The Progressive Intensity Hypothesis (Hypothesis 1) offers a simple yet powerful rule: weaker perturbations first, stronger ones later. Future works include investigating interference in more complex pipelines, providing explicit predictive rules, and automating compression order selection (see Appendix D.7).

540 REFERENCES
541

542 Saleh Ashkboos, Maximilian L Croci, Marcelo Gennari do Nascimento, Torsten Hoefer, and James
543 Hensman. Slicecpt: Compress large language models by deleting rows and columns. In *ICLR*,
544 2024a.

545 Saleh Ashkboos, Amirkeivan Mohtashami, Maximilian L Croci, Bo Li, Pashmina Cameron, Martin
546 Jaggi, Dan Alistarh, Torsten Hoefer, and James Hensman. Quarot: Outlier-free 4-bit inference in
547 rotated llms. In *NeurIPS*, 2024b.

548 Anonymous Authors. Supplementary materials (submitted). In *ICLR Submission*, 2026.

549 Yonatan Bisk, Rowan Zellers, Jianfeng Gao, Yejin Choi, et al. Piqa: Reasoning about physical
550 commonsense in natural language. In *AAAI*, 2020.

551 Daniel Cer, Mona Diab, Eneko Agirre, Iñigo Lopez-Gazpio, and Lucia Specia. Semeval-2017
552 task 1: Semantic textual similarity multilingual and crosslingual focused evaluation. In *Eleventh
553 International Workshop on Semantic Evaluation*, 2017.

554 Krishna Teja Chitty-Venkata, Sparsh Mittal, Murali Emani, Venkatram Vishwanath, and Arun K
555 Somani. A survey of techniques for optimizing transformer inference. *Journal of Systems
556 Architecture*, 144:102990, 2023.

557 Zheng Chuanyang, Zheyang Li, Kai Zhang, Zhi Yang, Wenming Tan, Jun Xiao, Ye Ren, and Shiliang
558 Pu. SAVit: Structure-aware vision transformer pruning via collaborative optimization. In *NeurIPS*,
559 2022.

560 Peter Clark, Isaac Cowhey, Oren Etzioni, Tushar Khot, Ashish Sabharwal, Carissa Schoenick, and
561 Oyvind Tafjord. Think you have solved question answering? try arc, the ai2 reasoning challenge.
562 *arXiv preprint arXiv:1803.05457*, 2018.

563 Pierre Vilar Dantas, Waldir Sabino da Silva Jr, Lucas Carvalho Cordeiro, and Celso Barbosa Car-
564 valho. A comprehensive review of model compression techniques in machine learning. *Applied
565 Intelligence*, 54(22):11804–11844, 2024.

566 J. Deng, W. Dong, R. Socher, L.-J. Li, K. Li, and L. Fei-Fei. Imagenet: A large-scale hierarchical
567 image database. In *CVPR*, 2009.

568 Lei Deng, Guoqi Li, Song Han, Luping Shi, and Yuan Xie. Model compression and hardware
569 acceleration for neural networks: A comprehensive survey. *Proceedings of the IEEE*, 108(4):
570 485–532, 2020.

571 Aditya Desai and Anshumali Shrivastava. In defense of parameter sharing for model-compression.
572 In *ICLR*, 2024.

573 Jacob Devlin, Ming-Wei Chang, Kenton Lee, and Kristina Toutanova. Bert: Pre-training of deep
574 bidirectional transformers for language understanding. In *NAACL*, 2019.

575 Zhen Dong, Zhewei Yao, Daiyaan Arfeen, Amir Gholami, Michael W Mahoney, and Kurt Keutzer.
576 Hawq-v2: Hessian aware trace-weighted quantization of neural networks. In *NeurIPS*, 2020.

577 Lizhe Fang, Yifei Wang, Zhaoyang Liu, Chenheng Zhang, Stefanie Jegelka, Jinyang Gao, Bolin Ding,
578 and Yisen Wang. What is wrong with perplexity for long-context language modeling? In *ICLR*,
579 2025.

580 Elias Frantar and Dan Alistarh. SparseGPT: Massive language models can be accurately pruned in
581 one-shot. In *ICML*, 2023.

582 Elias Frantar, Saleh Ashkboos, Torsten Hoefer, and Dan Alistarh. OPTQ: accurate quantization for
583 generative pre-trained transformers. In *ICLR*, 2023.

584 Amir Gholami, Sehoon Kim, Zhen Dong, Zhewei Yao, Michael W Mahoney, and Kurt Keutzer. A
585 survey of quantization methods for efficient neural network inference. In *Low-Power Computer
586 Vision*, pp. 291–326. Chapman and Hall/CRC, 2022.

594 Aaron Grattafiori, Abhimanyu Dubey, Abhinav Jauhri, Abhinav Pandey, Abhishek Kadian, Ahmad
 595 Al-Dahle, Aiesha Letman, Akhil Mathur, Alan Schelten, Alex Vaughan, et al. The llama 3 herd of
 596 models. *arXiv preprint arXiv:2407.21783*, 2024.

597

598 Suyog Gupta, Ankur Agrawal, Kailash Gopalakrishnan, and Pritish Narayanan. Deep learning with
 599 limited numerical precision. In *ICML*, 2015.

600 Song Han, Jeff Pool, John Tran, and William Dally. Learning both weights and connections for
 601 efficient neural network. In *NeurIPS*, 2015.

602

603 Simla Burcu Harma, Ayan Chakraborty, Elizaveta Kostenok, Danila Mishin, Dongho Ha, Babak
 604 Falsafi, Martin Jaggi, Ming Liu, Yunho Oh, Suvinay Subramanian, and Amir Yazdanbakhsh.
 605 Effective interplay between sparsity and quantization: From theory to practice. In *ICLR*, 2025.

606

607 Benjamin Hawks, Javier Duarte, Nicholas J Fraser, Alessandro Pappalardo, Nhan Tran, and Yaman
 608 Umuroglu. Ps and qs: Quantization-aware pruning for efficient low latency neural network
 609 inference. *Frontiers in Artificial Intelligence*, 4:676564, 2021.

610 Kaiming He, Xiangyu Zhang, Shaoqing Ren, and Jian Sun. Deep residual learning for image
 611 recognition. In *CVPR*, 2016.

612

613 Edward J Hu, yelong shen, Phillip Wallis, Zeyuan Allen-Zhu, Yuanzhi Li, Shean Wang, Lu Wang,
 614 and Weizhu Chen. LoRA: Low-rank adaptation of large language models. In *ICLR*, 2022.

615

616 Peng Hu, Xi Peng, Hongyuan Zhu, Mohamed M Sabry Aly, and Jie Lin. Opq: Compressing deep
 617 neural networks with one-shot pruning-quantization. In *AAAI*, 2021.

618

619 Sitao Huang, Carl Pearson, Rakesh Nagi, Jinjun Xiong, Deming Chen, and Wen-mei Hwu. Acceler-
 620 ating sparse deep neural networks on fpgas. In *HPEC*, 2019.

621

622 Albert Q. Jiang, Alexandre Sablayrolles, Arthur Mensch, Chris Bamford, Devendra Singh Chaplot,
 623 Diego de las Casas, Florian Bressand, et al. Mistral 7b. *arXiv preprint arXiv:2310.06825*, 2023.

624

625 Jangho Kim, Simyung Chang, and Nojun Kwak. Pqk: Model compression via pruning, quantization,
 626 and knowledge distillation. In *Interspeech*, 2021.

627

628 Minjun Kim, Jongjin Kim, and U Kang. SynQ: Accurate zero-shot quantization by synthesis-aware
 629 fine-tuning. In *ICLR*, 2025.

630

631 Eldar Kurtic, Daniel Campos, Tuan Nguyen, Elias Frantar, Mark Kurtz, Benjamin Fineran, Michael
 632 Goin, and Dan Alistarh. The optimal BERT surgeon: Scalable and accurate second-order pruning
 633 for large language models. In *EMNLP*, 2022.

634

635 Andrey Kuzmin, Markus Nagel, Mart Van Baalen, Arash Behboodi, and Tijmen Blankevoort. Pruning
 636 vs quantization: Which is better? In *NeurIPS*, 2023.

637

638 Changhun Lee, Jungyu Jin, Taesu Kim, Hyungjun Kim, and Eunhyeok Park. Owq: Outlier-aware
 639 weight quantization for efficient fine-tuning and inference of large language models. In *AAAI*,
 640 2024.

641

642 Muyang Li, Yujun Lin, Zhekai Zhang, Tianle Cai, Junxian Guo, Xiuyu Li, Enze Xie, Chenlin Meng,
 643 Jun-Yan Zhu, and Song Han. SVDQuant: Absorbing outliers by low-rank component for 4-bit
 644 diffusion models. In *ICLR*, 2025.

645

646 Yuhang Li, Ruihao Gong, Xu Tan, Yang Yang, Peng Hu, Qi Zhang, Fengwei Yu, Wei Wang, and Shi
 647 Gu. Brecq: Pushing the limit of post-training quantization by block reconstruction. In *ICLR*, 2021.

648

649 Zhikai Li, Junrui Xiao, Lianwei Yang, and Qingyi Gu. Repq-vit: Scale reparameterization for
 650 post-training quantization of vision transformers. In *ICCV*, 2023.

651

652 Tailin Liang, John Glossner, Lei Wang, Shaobo Shi, and Xiaotong Zhang. Pruning and quantization
 653 for deep neural network acceleration: A survey. *Neurocomputing*, 461:370–403, 2021.

648 Haokun Lin, Haobo Xu, Yichen Wu, Jingzhi Cui, Yingtao Zhang, Linzhan Mou, Linqi Song, Zhenan
 649 Sun, and Ying Wei. Duquant: Distributing outliers via dual transformation makes stronger quantized
 650 llms. In *NeurIPS*, 2024.

651

652 Defu Liu, Yixiao Zhu, Zhe Liu, Yi Liu, Changlin Han, Jinkai Tian, Ruihao Li, and Wei Yi. A survey
 653 of model compression techniques: Past, present, and future. *Frontiers in Robotics and AI*, 12:
 654 1518965, 2025a.

655

656 Zechun Liu, Kwang-Ting Cheng, Dong Huang, Eric P Xing, and Zhiqiang Shen. Nonuniform-to-
 657 uniform quantization: Towards accurate quantization via generalized straight-through estimation.
 658 In *CVPR*, 2022.

659

660 Zechun Liu, Changsheng Zhao, Igor Fedorov, Bilge Soran, Dhruv Choudhary, Raghuraman Krish-
 661 namoorthi, Vikas Chandra, Yuandong Tian, and Tijmen Blankevoort. Spinquant: Llm quantization
 662 with learned rotations. In *ICLR*, 2025b.

663

664 Zichang Liu, Jue Wang, Tri Dao, Tianyi Zhou, Binhang Yuan, Zhao Song, Anshumali Shrivastava,
 665 Ce Zhang, Yuandong Tian, Christopher Re, et al. Deja vu: Contextual sparsity for efficient llms at
 666 inference time. In *ICML*, 2023.

667

668 Sourab Mangrulkar, Sylvain Gugger, Lysandre Debut, Younes Belkada, Sayak Paul, and Benjamin
 669 Bossan. PEFT: State-of-the-art parameter-efficient fine-tuning methods. <https://github.com/huggingface/peft>, 2022.

670

671 Clara Meister and Ryan Cotterell. Language model evaluation beyond perplexity. In *ACL*, 2021.

672

673 Stephen Merity, Caiming Xiong, James Bradbury, and Richard Socher. Pointer sentinel mixture
 674 models. In *ICLR*, 2017.

675

676 Mistral AI Team. Mistral NeMo: our new best small model. <https://mistral.ai/news/mistral-nemo>, July 2024. Accessed: 2025.

677

678 Beatrice Alessandra Motetti, Matteo Risso, Alessio Burrello, Enrico Macii, Massimo Poncino, and
 679 Daniele Jahier Pagliari. Joint Pruning and Channel-Wise Mixed-Precision Quantization for Efficient
 680 Deep Neural Networks. *IEEE Transactions on Computers*, 73(11):2619–2633, 2024.

681

682 Azade Nova, Hanjun Dai, and Dale Schuurmans. Gradient-free structured pruning with unlabeled
 683 data. In *ICML*, 2023.

684

685 D Paperno, G Kruszewski, A Lazaridou, QN Pham, Raffaella Bernardi, S Pezzelle, M Baroni,
 686 G Boleda, and R Fernández. The lambada dataset: Word prediction requiring a broad discourse
 687 context. In *ACL*, 2016.

688

689 Seungcheol Park, Hojun Choi, and U Kang. Accurate retraining-free pruning for pretrained encoder-
 690 based language models. In *ICLR*, 2024.

691

692 Seungcheol Park, Jeongin Bae, Beomseok Kwon, Minjun Kim, Byeongwook Kim, Se Jung Kwon,
 693 U Kang, and Dongsoo Lee. Unifying uniform and binary-coding quantization for accurate
 694 compression of large language models. In *ACL*, 2025.

695

696 Xiaoyi Qu, David Aponte, Colby Banbury, Daniel P Robinson, Tianyu Ding, Kazuhito Koishida, Ilya
 697 Zharkov, and Tianyi Chen. Automatic joint structured pruning and quantization for efficient neural
 698 network training and compression. In *CVPR*, 2025.

699

700 Colin Raffel, Noam Shazeer, Adam Roberts, Katherine Lee, Sharan Narang, Michael Matena, Yanqi
 701 Zhou, Wei Li, and Peter J Liu. Exploring the limits of transfer learning with a unified text-to-text
 702 transformer. *Journal of machine learning research*, 21(140):1–67, 2020.

703

704 Keisuke Sakaguchi, Ronan Le Bras, Chandra Bhagavatula, and Yejin Choi. Winogrande: An adver-
 705 sarial winograd schema challenge at scale. *Communications of the ACM*, 64(9):99–106, 2021.

706

707 Tushar Shinde. Adaptive quantization and pruning of deep neural networks via layer importance
 708 estimation. In *Workshop on Machine Learning and Compression, NeurIPS 2024*, 2024.

702 Jiwon Song, Kyungseok Oh, Taesu Kim, Hyungjun Kim, Yulhwa Kim, and Jae-Joon Kim. Sleb:
 703 Streamlining llms through redundancy verification and elimination of transformer blocks. In *ICML*,
 704 2024.

705 Mingjie Sun, Zhuang Liu, Anna Bair, and J Zico Kolter. A simple and effective pruning approach for
 706 large language models. In *ICLR*, 2024.

708 Hugo Touvron, Matthieu Cord, Matthijs Douze, Francisco Massa, Alexandre Sablayrolles, and Hervé
 709 Jégou. Training data-efficient image transformers & distillation through attention. In *ICML*, 2021.

710 Hugo Touvron, Louis Martin, Kevin Stone, Peter Albert, Amjad Almahairi, Yasmine Babaei, Nikolay
 711 Bashlykov, Soumya Batra, Prajjwal Bhargava, Shruti Bhosale, et al. Llama 2: Open foundation
 712 and fine-tuned chat models. *arXiv preprint arXiv:2307.09288*, 2023.

713 Cuong Tran, Ferdinando Fioretto, Jung-Eun Kim, and Rakshit Naidu. Pruning has a disparate impact
 714 on model accuracy. In *NeurIPS*, 2022.

716 Albert Tseng, Jerry Chee, Qingyao Sun, Volodymyr Kuleshov, and Christopher De Sa. Quip#: Even
 717 better llm quantization with hadamard incoherence and lattice codebooks. In *ICML*, 2024.

718 Alex Wang, Amanpreet Singh, Julian Michael, Felix Hill, Omer Levy, and Samuel R. Bowman.
 719 GLUE: A multi-task benchmark and analysis platform for natural language understanding. In
 720 *ICLR*, 2019.

722 Guo-Hua Wang and Jianxin Wu. Practical network acceleration with tiny sets. In *CVPR*, 2023.

723 Jingcun Wang, Yu-Guang Chen, Ing-Chao Lin, Bing Li, and Grace Li Zhang. Basis sharing: Cross-
 724 layer parameter sharing for large language model compression. In *ICLR*, 2025a.

726 Naigang Wang, Chi-Chun Charlie Liu, Swagath Venkataramani, Sanchari Sen, Chia-Yu Chen, Kaoutar
 727 El Maghraoui, Vijayalakshmi Viji Srinivasan, and Leland Chang. Deep compression of pre-trained
 728 transformer models. In *NeurIPS*, 2022.

729 Tianzhe Wang, Kuan Wang, Han Cai, Ji Lin, Zhijian Liu, Hanrui Wang, Yujun Lin, and Song Han.
 730 Apq: Joint search for network architecture, pruning and quantization policy. In *CVPR*, 2020.

731 Xin Wang, Yu Zheng, Zhongwei Wan, and Mi Zhang. SVD-LLM: Truncation-aware singular value
 732 decomposition for large language model compression. In *ICLR*, 2025b.

734 Xiaoxia Wu, Cheng Li, Reza Yazdani Aminabadi, Zhewei Yao, and Yuxiong He. Understanding int4
 735 quantization for language models: latency speedup, composability, and failure cases. In *ICML*,
 736 2023.

737 Guangxuan Xiao, Ji Lin, Mickael Seznec, Hao Wu, Julien Demouth, and Song Han. Smoothquant:
 738 Accurate and efficient post-training quantization for large language models. In *ICML*, 2023.

740 Yi Xie, Huaidong Zhang, Xuemiao Xu, Jianqing Zhu, and Shengfeng He. Towards a smaller student:
 741 Capacity dynamic distillation for efficient image retrieval. In *CVPR*, 2023.

742 Canwen Xu and Julian McAuley. A survey on model compression and acceleration for pretrained
 743 language models. In *AAAI*, 2023.

744 Kaixin Xu, Zhe Wang, Chunyun Chen, Xue Geng, Jie Lin, Xulei Yang, Min Wu, Xiaoli Li, and Weisi
 745 Lin. Lpvit: Low-power semi-structured pruning for vision transformers. In *ECCV*, 2024.

747 Chong Yu, Tao Chen, Zhongxue Gan, and Jiayuan Fan. Boost vision transformer with gpu-friendly
 748 sparsity and quantization. In *CVPR*, 2023.

749 Rowan Zellers, Ari Holtzman, Yonatan Bisk, Ali Farhadi, and Yejin Choi. Hellaswag: Can a machine
 750 really finish your sentence? In *ACL*, 2019.

751 Pengxiang Zhao and Xiaoming Yuan. GANQ: GPU-adaptive non-uniform quantization for large
 752 language models. In *ICML*, 2025.

754 Xunyu Zhu, Jian Li, Yong Liu, Can Ma, and Weiping Wang. A survey on model compression for large
 755 language models. *Transactions of the Association for Computational Linguistics*, 12:1556–1577,
 2024.

A NOTATION

We summarize the frequently used notations in the paper as Table 2.

Table 2: Frequently used notations.

Symbol	Description
ϕ	A pre-trained model
ϕ'	A compressed model
$f(\cdot) \in \mathbb{F}$	Compression method from a set \mathbb{F}
C	Compression ratio
$\mathcal{M}(\cdot)$	Performance metric
$\mathbf{W}_i, \mathbf{X}_i$	Weight and activation matrices of layer l_i , respectively
$\pi \in \Pi$	Compression order from a set Π of all possible permutations
$\mathcal{P}(\cdot), \mathcal{Q}(\cdot)$	Pruning and quantization methods, respectively
p	Pruning ratio ($C_{\mathcal{P}} = 1/(1-p)$)
B_{orig}, B_Q	Original and quantized bit-widths, respectively
$\delta_f(\cdot)$	Error induced by applying $f(\cdot)$
$t \in \mathcal{T}_\phi$	Abstract data type from the set of all valid types in model ϕ
t_f	Granularity of $f(\cdot)$
$u \in \mathbb{U}(\phi; t)$	A unit of type t within the model ϕ
$\mathbb{D}_u^f(\pi)$	Binary indicator of whether $f(\cdot)$ modifies unit u under order π
$\mathcal{G}(f_1, f_2)$	Performance gap between $f_1(\cdot)$ and $f_2(\cdot)$
$\mathcal{A}(f_1 \rightarrow f_2)$	Compression order advantage of $f_1 \rightarrow f_2$ over $f_2 \rightarrow f_1$
C_f^*	Compression Equivalent Ratio (CER) of $f(\cdot)$
$\Delta(\phi; f_1 \rightarrow f_2)$	Interference from $f_1(\cdot)$ to $f_2(\cdot)$

B DETAILS ON THEORETICAL ANALYSIS

We provide the detailed proofs for Theorems 1 and 2, then formulate a generalized version of Hypothesis 1 applicable to a broader setting with multiple compression methods.

B.1 PROOF OF THEOREM 1

Proof. Given two compression methods $f_1(\cdot)$ and $f_2(\cdot)$ with respective granularities t_{f_1} and t_{f_2} , disjoint selectivity ensures that every unit is assigned exclusively to one method. Hence, every unit $u \in \mathbb{U}(\phi; t_{\text{lut}}(t_{f_1}, t_{f_2}))$ is classified into one of four disjoint groups, $\mathbb{G}_1, \mathbb{G}_2, \mathbb{G}_3$, or \mathbb{G}_4 , according to its assigned method. Then,

$$\begin{aligned}\mathbb{G}_1 &= \{u \mid \mathbb{D}_u^{f_1}(f_2 \circ f_1) = 1, \mathbb{D}_u^{f_1}(f_1 \circ f_2) = 0\}, \\ \mathbb{G}_2 &= \{u \mid \mathbb{D}_u^{f_1}(f_2 \circ f_1) = 0, \mathbb{D}_u^{f_1}(f_1 \circ f_2) = 1\}, \\ \mathbb{G}_3 &= \{u \mid \mathbb{D}_u^{f_1}(f_2 \circ f_1) = 0, \mathbb{D}_u^{f_1}(f_1 \circ f_2) = 0\}, \\ \mathbb{G}_4 &= \{u \mid \mathbb{D}_u^{f_1}(f_2 \circ f_1) = 1, \mathbb{D}_u^{f_1}(f_1 \circ f_2) = 1\}, \\ \mathbb{G}_1 \cup \mathbb{G}_2 \cup \mathbb{G}_3 \cup \mathbb{G}_4 &= \mathbb{U}(\phi; t_{\text{lut}}(t_{f_1}, t_{f_2})),\end{aligned}$$

where $\mathbb{U}(\phi; t)$ represents the unit set of model ϕ at granularity t , and $\mathbb{D}_u^f(\pi)$ records whether $f(\cdot)$ modifies u under the ordering π (1 if yes, 0 if no). Note that these four groups are mutually exclusive and collectively exhaustive. Also, $|\mathbb{G}_1| = |\mathbb{G}_2|$ since the compression ratio $C_{\mathcal{P}}$ is identical regardless of the compression order. Figure 11 illustrates the four groups.

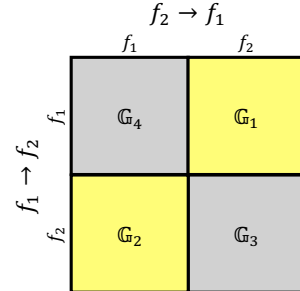


Figure 11: We partition all units u into four disjoint groups. Only groups \mathbb{G}_1 and \mathbb{G}_2 influence $\mathcal{A}(f_1 \rightarrow f_2)$.

Under Assumption 1 and the defined partitioning of groups, the compression order advantage $\mathcal{A}(\cdot)$ is expressed in terms of unit-wise reconstruction errors $\delta_f(u_i)$:

$$\begin{aligned}
& \mathcal{A}(f_1 \rightarrow f_2) \\
&= \mathcal{M}((f_2 \circ f_1)(\phi)) - \mathcal{M}((f_1 \circ f_2)(\phi)) \\
&= -\beta(\delta_{(f_2 \circ f_1)}(\phi) - \delta_{(f_1 \circ f_2)}(\phi)) \\
&= -\beta \left(\sum_{u_i \in \mathbb{G}_1} \|\delta_{f_1}(u_i)\|_F^2 + \sum_{u_i \in \mathbb{G}_2} \|\delta_{f_2}(u_i)\|_F^2 + \sum_{u_i \in \mathbb{G}_3} \|\delta_{f_2}(u_i)\|_F^2 + \sum_{u_i \in \mathbb{G}_4} \|\delta_{f_1}(u_i)\|_F^2 \right. \\
&\quad \left. - \sum_{u_i \in \mathbb{G}_1} \|\delta_{f_2}(u_i)\|_F^2 - \sum_{u_i \in \mathbb{G}_2} \|\delta_{f_1}(u_i)\|_F^2 - \sum_{u_i \in \mathbb{G}_3} \|\delta_{f_2}(u_i)\|_F^2 - \sum_{u_i \in \mathbb{G}_4} \|\delta_{f_1}(u_i)\|_F^2 \right) \\
&= -\beta \left(\sum_{u_i \in \mathbb{G}_1} \|\delta_{f_1}(u_i)\|_F^2 + \sum_{u_i \in \mathbb{G}_2} \|\delta_{f_2}(u_i)\|_F^2 - \sum_{u_i \in \mathbb{G}_1} \|\delta_{f_2}(u_i)\|_F^2 - \sum_{u_i \in \mathbb{G}_2} \|\delta_{f_1}(u_i)\|_F^2 \right) \\
&= \beta \left(\sum_{u_i \in \mathbb{G}_2} g(u_i) - \sum_{u_i \in \mathbb{G}_1} g(u_i) \right),
\end{aligned}$$

where error difference $g(u_i) = \|\delta_{f_1}(u_i)\|_F^2 - \|\delta_{f_2}(u_i)\|_F^2$. Note that \mathbb{G}_3 and \mathbb{G}_4 are discarded since their effect remains unchanged irrespective of the compression order. \square

Case study on pruning and quantization. To support intuition, we provide a case study on pruning and quantization, which constitute the core scenario of our work. As described in the main text, disjoint selectivity holds only when the granularity $t_{\mathcal{P}}$ of pruning $\mathcal{P}(\cdot)$ is greater than or equal to the granularity $t_{\mathcal{Q}}$ of quantization $\mathcal{Q}(\cdot)$. We analyze this at the layer level: let \mathbf{W}_i and \mathbf{X}_i denote the weight and activation of a layer $l_i \in \mathbb{L}$ in the model ϕ . Note that the error $\delta_f(\mathbf{W}_i, \mathbf{X}_i) = f(\mathbf{W}_i)f(\mathbf{X}_i) - \mathbf{W}_i\mathbf{X}_i$ for a compression method $f(\cdot)$, as described in Section 2.

We partition the layers \mathbb{L} into four disjoint groups $\mathbb{G}_1, \mathbb{G}_2, \mathbb{G}_3$, and \mathbb{G}_4 based on their pruning status:

$$\begin{aligned}
\mathbb{G}_1 &= \mathbb{P}_{\mathcal{Q} \circ \mathcal{P}} \setminus \mathbb{P}_{\mathcal{P} \circ \mathcal{Q}}, \\
\mathbb{G}_2 &= \mathbb{P}_{\mathcal{P} \circ \mathcal{Q}} \setminus \mathbb{P}_{\mathcal{Q} \circ \mathcal{P}}, \\
\mathbb{G}_3 &= \mathbb{P}_{\mathcal{Q} \circ \mathcal{P}} \cap \mathbb{P}_{\mathcal{P} \circ \mathcal{Q}}, \\
\mathbb{G}_4 &= \mathbb{L} \setminus (\mathbb{P}_{\mathcal{Q} \circ \mathcal{P}} \cup \mathbb{P}_{\mathcal{P} \circ \mathcal{Q}}), \\
\mathbb{G}_1 \cup \mathbb{G}_2 \cup \mathbb{G}_3 \cup \mathbb{G}_4 &= \mathbb{L},
\end{aligned}$$

where \mathbb{P}_f denote the sets of pruned layers when applying $f(\cdot)$.

Then, the quantization-first advantage $\mathcal{A}(\mathcal{Q} \rightarrow \mathcal{P})$ is estimated as follows:

$$\begin{aligned}
\mathcal{A}(\mathcal{Q} \rightarrow \mathcal{P}) &= \mathcal{M}((\mathcal{P} \circ \mathcal{Q})(\phi)) - \mathcal{M}((\mathcal{Q} \circ \mathcal{P})(\phi)) = -\beta(\delta_{\mathcal{P} \circ \mathcal{Q}}(\phi) - \delta_{\mathcal{Q} \circ \mathcal{P}}(\phi)) \\
&= -\beta \left(\sum_{l_i \in \mathbb{L}} \|\delta_{\mathcal{P} \circ \mathcal{Q}}(\mathbf{W}_i, \mathbf{X}_i)\|_F^2 - \|\delta_{\mathcal{Q} \circ \mathcal{P}}(\mathbf{W}_i, \mathbf{X}_i)\|_F^2 \right) \\
&= -\beta \left(\sum_{l_i \in \mathbb{L}} \|\delta_{\mathcal{P}}(\mathcal{Q}(\mathbf{W}_i), \mathcal{Q}(\mathbf{X}_i)) + \delta_{\mathcal{Q}}(\mathbf{W}_i, \mathbf{X}_i)\|_F^2 - \|\delta_{\mathcal{Q}}(\mathcal{P}(\mathbf{W}_i), \mathcal{P}(\mathbf{X}_i)) + \delta_{\mathcal{P}}(\mathbf{W}_i, \mathbf{X}_i)\|_F^2 \right) \\
&= -\beta \left(\sum_{l_i \in \mathbb{G}_1} \left\{ \|\delta_{\mathcal{Q}}(\mathbf{W}_i, \mathbf{X}_i)\|_F^2 - \|-\mathbf{W}_i\mathbf{X}_i\|_F^2 \right\} \right. \\
&\quad \left. + \sum_{l_i \in \mathbb{G}_2} \left\{ \|\delta_{\mathcal{Q}}(\mathbf{W}_i, \mathbf{X}_i) + \delta_{\mathcal{Q}}(\mathbf{W}_i, \mathbf{X}_i)\|_F^2 - \|\delta_{\mathcal{Q}}(\mathbf{W}_i, \mathbf{X}_i)\|_F^2 \right\} \right) \\
&= -\beta \left(\sum_{l_i \in \mathbb{G}_1} \left\{ \|\delta_{\mathcal{Q}}(\mathbf{W}_i, \mathbf{X}_i)\|_F^2 - \|-\mathbf{W}_i\mathbf{X}_i\|_F^2 \right\} + \sum_{l_i \in \mathbb{G}_2} \left\{ \|-\mathbf{W}_i\mathbf{X}_i\|_F^2 - \|\delta_{\mathcal{Q}}(\mathbf{W}_i, \mathbf{X}_i)\|_F^2 \right\} \right) \\
&= \beta \left(\sum_{l_i \in \mathbb{G}_2} g(\mathbf{W}_i, \mathbf{X}_i) - \sum_{l_i \in \mathbb{G}_1} g(\mathbf{W}_i, \mathbf{X}_i) \right),
\end{aligned}$$

864 where $g(\mathbf{W}_i, \mathbf{X}_i) = \|\delta_{\mathcal{Q}}(\mathbf{W}_i, \mathbf{X}_i)\|_F^2 - \|-\mathbf{W}_i \mathbf{X}_i\|_F^2$. This expression holds as for any layer $l_i \in \mathbb{L}$,
 865 the pruning operator and its associated error are defined as follows:
 866

$$867 \quad \mathcal{P}(\mathbf{W}_i)\mathcal{P}(\mathbf{X}_i) = \begin{cases} \mathbf{0} & \text{if pruned} \\ \mathbf{W}_i \mathbf{X}_i & \text{otherwise} \end{cases}, \quad \delta_{\mathcal{P}}(\mathbf{W}_i, \mathbf{X}_i) = \begin{cases} -\mathbf{W}_i \mathbf{X}_i & \text{if pruned} \\ \mathbf{0} & \text{otherwise} \end{cases}.$$

870 **B.2 PROOF OF THEOREM 2**

872 *Proof.* As $\mathcal{A}(\mathcal{Q} \rightarrow \mathcal{P})$ and $\mathcal{G}(\cdot)$ (or $C_{\mathcal{P}}^* - C_{\mathcal{Q}}$) are functions of the compression ratio $C_{\mathcal{Q}}$ we analyze
 873 their behavior separately. Without loss of generality, we consider only the case where each ratio
 874 changes in the direction of increasing $C_{\mathcal{P}}^* - C_{\mathcal{Q}}$, i.e., decreasing $C_{\mathcal{Q}}$.

875 Under Assumption 2, which assumes well-designed quantization, decreasing $C_{\mathcal{Q}}$ preserves the
 876 expected value of the quantized outputs while decreasing their standard deviation. As pruning
 877 intensity is held constant, the variation across compression orders is attributed solely to the severity
 878 of quantization. Lower quantization ratio (i.e., smaller standard deviation) decreases the chance that
 879 units behave differently across orders, which can only decrease or preserve the value of $|\mathbb{G}_1| = |\mathbb{G}_2|$,
 880 but never increase it. We analyze the two possible cases as follows.

- 881 **Case 1: Number of layers affected by order decreases.** Although more than one layer may
 882 change simultaneously, any such change can be decomposed into a sequence in which layers are
 883 added one by one; thus it suffices to analyze the case where exactly one layer is added. Let l_i and
 884 l_j denote the layers moving from \mathbb{G}_1 and \mathbb{G}_2 to \mathbb{G}_3 , respectively. As only \mathbb{G}_1 and \mathbb{G}_2 contribute to
 885 $\mathcal{A}(\mathcal{Q} \rightarrow \mathcal{P})$, this value will not decrease if $g(l_j) - g(l_i) \leq 0$. The loss is given as:

$$886 \quad g(l_j) - g(l_i) = (\|\delta_{\mathcal{Q}}(\mathbf{W}_j, \mathbf{X}_j)\|_F^2 - \|\delta_{\mathcal{Q}}(\mathbf{W}_i, \mathbf{X}_i)\|_F^2) - (\|-\mathbf{W}_j \mathbf{X}_j\|_F^2 - \|-\mathbf{W}_i \mathbf{X}_i\|_F^2).$$

888 Under Assumptions 1 and 2, the second term in parentheses is positive, i.e., $\|-\mathbf{W}_j \mathbf{X}_j\|_F^2 - \|-\mathbf{W}_i \mathbf{X}_i\|_F^2 > 0$. This is because under pruning alone, $l_i \in \mathbb{G}_1$ is pruned while $l_j \in \mathbb{G}_2$ is not. Under
 889 the well-designed pruning assumption, which minimizes performance drop, Assumption 1 implies
 890 that this is equivalent to minimizing error increase. Therefore, the pruning error $\|-\mathbf{W}_i \mathbf{X}_i\|_F^2$ for
 891 pruned l_i is less than or equal to $\|-\mathbf{W}_j \mathbf{X}_j\|_F^2$ for unpruned l_j , making the term positive.

893 Given the assumption of well-designed quantization in Assumption 2, the remaining first term,
 894 which denotes the difference in quantization errors, is negligible compared to the pruning-related
 895 component. This is because the quantization error at each layer is modeled as zero-mean noise with
 896 small variance, whereas the pruning error term $\|-\mathbf{W}_i \mathbf{X}_i\|_F^2$ (or $\|-\mathbf{W}_j \mathbf{X}_j\|_F^2$) corresponds directly
 897 to the magnitude of the pruned responses. Thus, the difference $\|\delta_{\mathcal{Q}}(\mathbf{W}_j, \mathbf{X}_j)\|_F^2 - \|\delta_{\mathcal{Q}}(\mathbf{W}_i, \mathbf{X}_i)\|_F^2$
 898 remains uniformly small compared to $\|-\mathbf{W}_j \mathbf{X}_j\|_F^2 - \|-\mathbf{W}_i \mathbf{X}_i\|_F^2$, so the pruning-induced gap
 899 dominates $g(l_j) - g(l_i)$. Consequently, we get

$$900 \quad g(l_j) - g(l_i) \approx -(\|-\mathbf{W}_j \mathbf{X}_j\|_F^2 - \|-\mathbf{W}_i \mathbf{X}_i\|_F^2) < 0.$$

902 Overall, as the decrease in number of order-dependent layers eliminates negative loss term, com-
 903 pression order advantage $\mathcal{A}(\mathcal{Q} \rightarrow \mathcal{P})$ increases.

- 904 **Case 2: Number of layers affected by order remains unchanged.** As the loss-contributing groups
 905 \mathbb{G}_1 and \mathbb{G}_2 do not change, the compression order advantage $\mathcal{A}(\mathcal{Q} \rightarrow \mathcal{P})$ remains unaffected.

907 In conclusion, monotonicity holds under fixed $C_{\mathcal{P}}$ as $\mathcal{A}(\mathcal{Q} \rightarrow \mathcal{P})$ does not decrease in the direction
 908 where $C_{\mathcal{P}}^* - C_{\mathcal{Q}}$ increases. \square

910 **B.3 GENERALIZATION TO MULTIPLE METHODS**

912 We formulate Hypothesis 1 in the main text under the setting of two compression methods $f_1(\cdot)$ and
 913 $f_2(\cdot)$. This is because if the hypothesis holds for any pair of methods, it can be generalized to more
 914 than two methods.

915 Following the setup in Problem 1, suppose we sequentially apply a set $\mathbb{F} = f_1(\cdot), f_2(\cdot), \dots, f_n(\cdot)$
 916 of compression methods to a pre-trained model ϕ . Then, any pair (π_1, π_2) of permutations from
 917 the set $\Pi = \{\pi : \mathbb{F} \rightarrow \mathbb{F} \mid \pi \text{ is bijective}\}$ of all permutations can be converted into one another via
 a sequence of adjacent transpositions. This is because the adjacent transpositions generate the full

Table 3: Baseline methods covered in our experiments across different settings.

Compression	Modality	Target Models	Baseline Methods
Pruning $\mathcal{P}(\cdot)$	Language models	Decoder-only models	SparseGPT (Frantar & Alistarh, 2023), Wanda (Sun et al., 2024), SLEB (Song et al., 2024)
		Encoder-based models	K-prune (Park et al., 2024)
	Vision models	CNNs	PRACTISE (Wang & Wu, 2023)
		ViTs	SAViT (Chuanyang et al., 2022)
	Language models	Decoder-only models	RTN (Gupta et al., 2015), OPTQ (Frantar et al., 2023), QuaRoT (Ashkboos et al., 2024b)
		Encoder-based models	UniQuanF (Park et al., 2025)
		CNNs	N2UQ (Liu et al., 2022)
		ViTs	RepQ-ViT (Li et al., 2023)
Parameter Efficient Fine-tuning	Language models	Decoder-only models	LoRA (Hu et al., 2022)
Parameter Sharing	Language models	Decoder-only models	Basis Sharing (Wang et al., 2025a)
Mixed-precision quantization	Vision models	CNNs	HAWQ-V2 (Dong et al., 2020)

947 symmetric group, allowing any permutation to be constructed from another. Thus, under Hypothesis 1,
948 we demonstrate our original claim in Figure 1 that applying stronger permutations later leads to better
949 performance or the compressed model.

C EXPERIMENTAL SETUP

953 We describe the details on the experimental setup, including models, datasets, baselines, evaluation
954 protocol, and implementation.

955 **Models.** We evaluate representative models across modalities, including LLaMA 2 (7B, 13B) (Tou-
956 vron et al., 2023), LLaMA 3 8B (Grattafiori et al., 2024), Mistral 7B (Jiang et al., 2023), Mistral
957 Nemo-12B (Mistral AI Team, 2024), and BERT (Devlin et al., 2019) for language, and ResNet-18 (He
958 et al., 2016) and DeiT-Base (Touvron et al., 2021) for vision.

959 **Datasets.** We evaluate decoder-only language models on WikiText-2 (Merity et al., 2017) and C4 (Raf-
960 fel et al., 2020) datasets for perplexity, and on five commonsense reasoning tasks—ARC (Clark
961 et al., 2018), HellaSwag (Zellers et al., 2019), LAMBADA (Paperno et al., 2016), PIQA (Bisk et al.,
962 2020), and Winogrande (Sakaguchi et al., 2021). For encoder-based models, we evaluate performance
963 using the Spearman’s rank correlation coefficient on the STS-B dataset. For vision models, we report
964 classification accuracy on the ImageNet (ILSVRC 2012) (Deng et al., 2009) dataset.

965 **Baseline Methods.** We validate our hypothesis across a total of sixteen pairs of compression methods
966 by incorporating six pruning methods, six quantization methods, and one mixed-precision quantiza-
967 tion method. Table 3 provides an overview of baseline methods categorized by target models and
968 modalities. Refer to the original papers for further details.

969 **Evaluation Protocol.** The calibration dataset consists of a single batch with 128 samples drawn from
970 the same dataset used for perplexity evaluation. We set the batch size to 16 for perplexity evaluation
971 and to 128 for commonsense reasoning tasks. All quantization methods apply the same bit-width to

972 weights, activations, and KV-cache, with clipping applied during weight quantization. Both models
 973 are evaluated without fine-tuning using a batch size of 128. Metrics are reported as the average of five
 974 repeated runs, each computed with four-digit precision. We plot the relative values for visualization.
 975

976 **Implementation and Machine.** Our implementations are written in Python and rely on PyTorch,
 977 Transformers, Accelerate, and TorchVision libraries. For all baseline methods, we reproduce the
 978 results based on their open-source code and hyperparameter configurations. All of our experiments
 979 are done at a workstation with Intel Xeon Gold 6338 and NVIDIA A100 80GB.
 980

981 **Parameter Efficient Fine-tuning Experiment.** We adopt LoRA (Hu et al., 2022) on top of
 982 SparseGPT (Frantar & Alistarh, 2023) and RTN (Gupta et al., 2015) to fine-tune the compressed
 983 model. The target model is LLaMA 3 8B (Grattafiori et al., 2024), where fine-tuning is processed
 984 after quantization. We select WikiText-2 as the calibration dataset and train for a total of 2 epochs.
 985 We follow Basis Sharing (Wang et al., 2025a) for training details of the low-rank adapter, while
 986 exploiting the PEFT (Mangrulkar et al., 2022) library.
 987

988 **Parameter Sharing Experiment.** We evaluate the performance of a LLaMA 2 7B model when
 989 applying Basis Sharing (Wang et al., 2025a) and magnitude-based pruning (Han et al., 2015). We
 990 follow Basis Sharing for hyperparameters regarding parameter sharing, where the group size is 128.
 991 QuaRot (Ashkboos et al., 2024b) is selected as the quantization baseline for calculating compression
 992 equivalent bits. No additional fine-tuning is applied under this setting.
 993

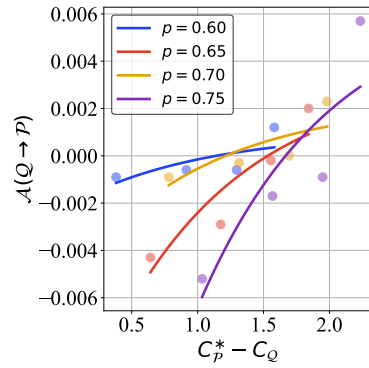
994 **Mixed-precision Quantization Experiment.** We base our method on HAWQ-V2 (Dong et al.,
 995 2020), but allocate bit-widths iteratively rather than in a single shot. At each iteration, we search
 996 per-layer bit-widths from a range of $[2, 3, 4, 5, 6, 7, 8]$ and train for 5 epochs. All other experimental
 997 settings, including hyperparameters and quantization techniques, are aligned with the original paper.
 998 We run all MPQ experiments on a workstation with Intel Xeon Silver 4310 and NVIDIA RTX 4090.
 999

1000 D FURTHER DISCUSSION AND EXPERIMENTS

1001 We present results from extended experiments and offer further discussion and remarks on our work.
 1002

1003 D.1 ANALYSIS ON ENCODER-BASED MODELS

1004 Beyond decoder-only LLMs, we extend our analysis to
 1005 encoder-based language models to validate the generality
 1006 of our hypothesis. Figure 12 presents the performance of
 1007 a BERT (Devlin et al., 2019) model under K-prune (Park
 1008 et al., 2024) ($\mathcal{P}(\cdot)$) and UniQuanF (Park et al., 2025) ($\mathcal{Q}(\cdot)$).
 1009 We adopt Spearman correlation as the performance metric,
 1010 measured on the STS-B dataset (Cer et al., 2017) from the
 1011 GLUE (Wang et al., 2019) benchmark. We have two observa-
 1012 tions from the result. First, we observe a monotonic increase
 1013 along both axes, confirming that our hypothesis holds. Nota-
 1014 bly, similar to our other findings, the fitted curve shows an
 1015 exponential pattern, indicating that performance differences
 1016 grow exponentially with compression ratio regardless of the
 1017 metric $\mathcal{M}(\cdot)$. Notably, the presence of positive advantage is
 1018 more consistent here, which is rarely seen in decoder-based
 1019 language models. This is because large $C_{\mathcal{P}}^* - C_{\mathcal{Q}}$ indicates
 1020 severe pruning-induced degradation, yet encoder-based models
 1021 remain robust even under additional quantization in those regions—unlike decoder-only models. This
 1022 suggests that the common belief in decoder-based LLMs—that pruning followed by quantization is
 1023 always better (Yu et al., 2023; Frantar & Alistarh, 2023; Harma et al., 2025)—likely stems from the
 1024 fact that pruning methods for LLMs still cause much greater degradation than quantization under
 1025 identical compression ratios, making the region where $\mathcal{A}(\mathcal{Q} \rightarrow \mathcal{P}) > 0$ harder to observe.



1026 Figure 12: The hypothesis holds
 1027 for encoder-based language models.
 1028 See Appendix D.1 for details.
 1029

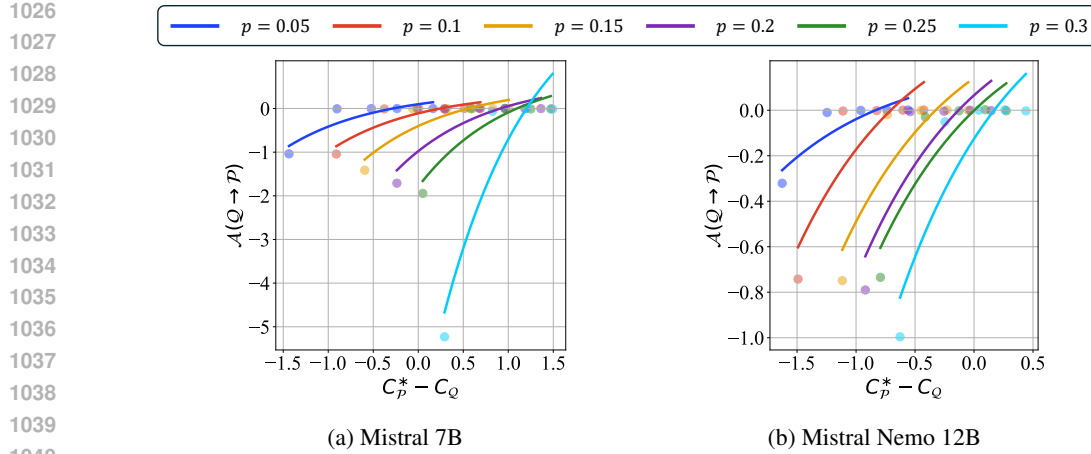


Figure 13: The compression order advantage $\mathcal{A}(Q \rightarrow P)$ increases monotonically with the CER difference $C_P^* - C_Q$ also for Mistral herd models. See Appendix D.2 for details.

D.2 EXPERIMENTS ON DIVERSE LLMs

Our experiments on decoder-only models are limited to the LLaMA herd (LLaMA 2 (Touvron et al., 2023), LLaMA 3 (Grattafiori et al., 2024)), which may not fully reflect broader generality. To address this, we conduct additional experiments on models from the Mistral herd. Figure 13 presents the results of applying SparseGPT ($\mathcal{P}(\cdot)$) and QuaRot ($\mathcal{Q}(\cdot)$) to Mistral 7B (Jiang et al., 2023) and Mistral Nemo 12B (Mistral AI Team, 2024). We have two observations from the result. First, the compression-order trend aligns well with the hypothesis across Mistral-based models. The result serves as additional evidence confirming the hypothesis in decoder-only language models. Second, comparing models within the same herd (see Figure 3), we find that smaller models exhibit greater variation in compression-order advantage for identical CER differences. This may be due to the fact that low-bit quantization (or stronger quantization) causes greater degradation in smaller models, intensifying observed differences.

D.3 COMMONSENSE REASONING PERFORMANCE

Although the negative of perplexity serves as an intuitive and efficient metric $\mathcal{M}(\cdot)$ for evaluating language models, prior studies (Meister & Cotterell, 2021; Fang et al., 2025) suggest it does not always correlate with real-world performance. We thus investigate the performance of a LLaMA 3 8B model across five commonsense reasoning tasks in Figure 14, under SparseGPT ($\mathcal{P}(\cdot)$) and QuaRot ($\mathcal{Q}(\cdot)$). Results affirm the generality and metric-agnostic nature of our framework, as the hypothesis holds across these tasks.

D.4 IMPACT OF ROTATION ON PRUNING METHODS

In Figure 5 and Finding 3, we observe that applying rotation without quantization may lead in notable degradation on pruning performance. To further analyze this, Table 4 compares the performance of a LLaMA 3 8B model pruned with and without QuaRot-based rotation, across two pruning methods with different granularities. We have two observations from the result. First, rotation-induced degradation scales with the pruning ratio. This is because higher pruning ratios result in more units being pruned that are altered by rotation, thereby increasing the error. Second, unstructured pruning exhibits significantly higher error compared to structured pruning. This trend is especially evident under high pruning ratios.

We therefore investigate the underlying reason behind this phenomenon. We identify two types of errors induced by pruning, depending on its granularity: matrix-wise and instance-wise. Figure 15 conceptually illustrates these two cases.

First, in the case of matrix-wise pruning, ignoring rotation during pruning leaves the rotation-induced matrix \mathbf{H} intact, introducing extra computation and numerical errors compared to the non-rotated case.

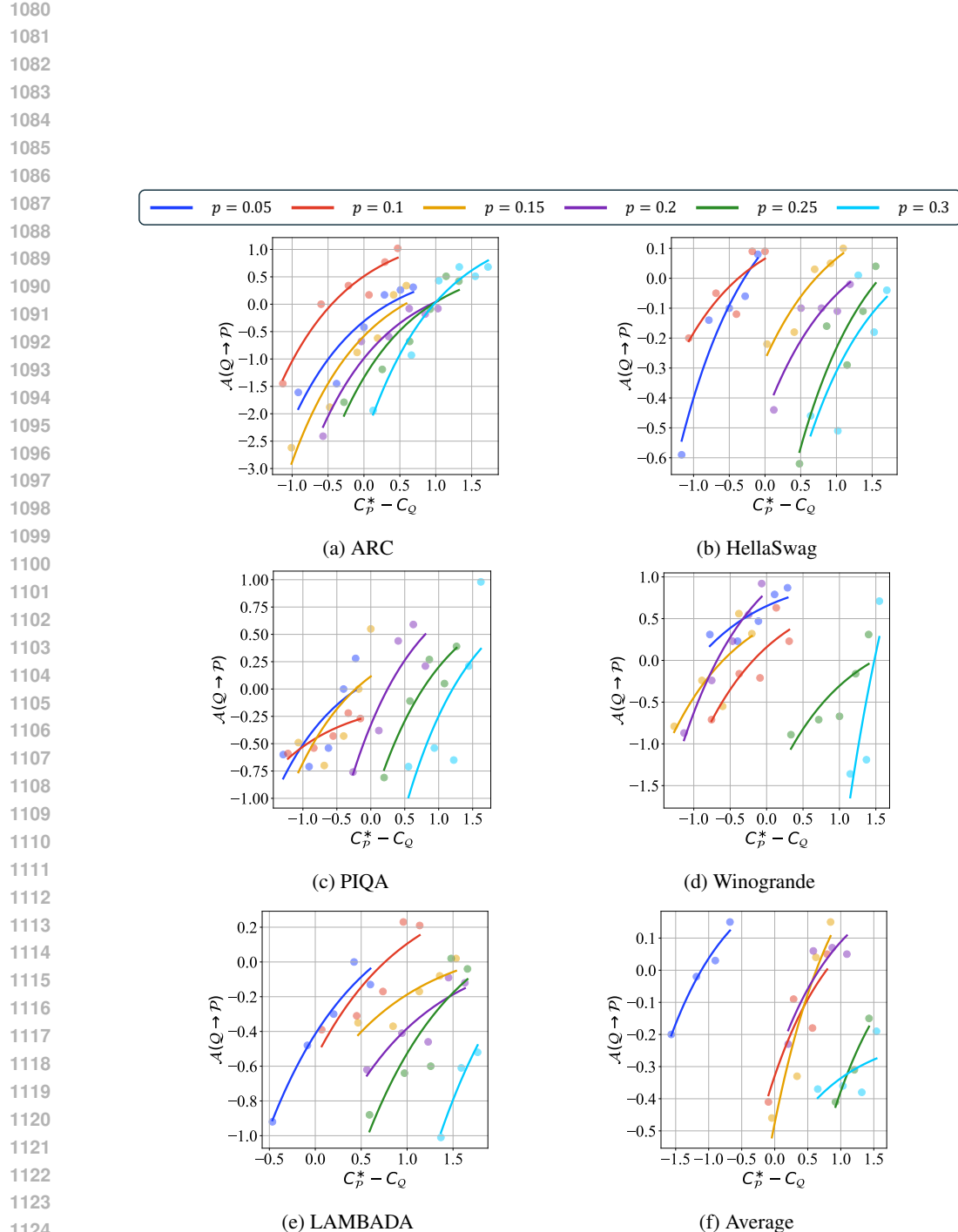


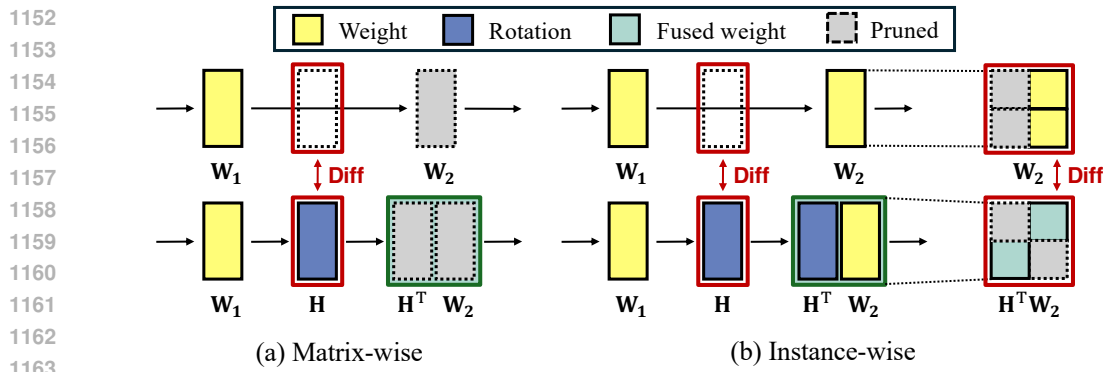
Figure 14: Commonsense reasoning task performance of a LLaMA 3 8B model for SparseGPT and QuaRot. See Appendix D.3 for details.

1134 Table 4: WikiText-2 perplexity comparison of a LLaMA 3 8B model pruned by SLEB (Song et al.,
 1135 2024) and SparseGPT (Frantar & Alistarh, 2023) under varying pruning ratios, with and without
 1136 rotation following QuaRot (Ashkboos et al., 2024b). See Section D.4 for details.

1137

1138 1139 1140 1141 1142 1143 1144 1145 1146 1147 1148 1149 1150	1138 1139 1140 1141 1142 1143 1144 1145 1146 1147 1148 1149 1150			1138 1139 1140 1141 1142 1143 1144 1145 1146 1147 1148 1149 1150			
	Pruning Ratio	No rotation	Rotation	Difference	No rotation	Rotation	Difference
Original				6.137			
0.05	6.857	6.871	0.014	6.140	6.154	0.014	
0.1	8.792	8.828	0.036	6.159	6.205	0.046	
0.15	12.603	12.615	0.012	6.213	6.352	0.139	
0.2	25.289	25.295	0.006	6.330	6.629	0.299	
0.25	51.212	51.560	0.348	6.546	7.250	0.704	
0.3	61.502	61.901	0.399	6.894	8.504	1.610	
0.35	65.997	66.234	0.237	7.474	20.842	13.368	
0.4	92.848	93.260	0.412	8.477	98.213	89.736	

1151



1163

Figure 15: Two cases of errors when pruning rotated units. See Section D.4 for details.

1164

1166 As suggested in QuaRot (Ashkboos et al., 2024b), the rotation inverse is fused into the target layer,
 1167 while the original transform is merged into the preceding normalization layer, leaving un-removed
 1168 components that generate error during naïve pruning. This type of error scales proportionally with
 1169 the pruning ratio, as each pruned matrix introduces one such error.

1170

1171 Second, in instance-wise pruning, additional errors arise due to rotation-induced changes in unit
 1172 selection, on top of the matrix-wise error. As the goal of rotation is to facilitate quantization by
 1173 flattening activation outliers, multiplying its inverse results in an error compared to the original matrix.
 1174 Consequently, the discrepancy in layer content leads to different pruning decisions. Furthermore, this
 1175 selection-based error grows with higher pruning ratios due to a greater number of pruned units.

1176

1176 In summary, given these errors, it is crucial to develop pruning techniques that align with rotation-
 1177 based quantization strategies.

1178

1179 D.5 A DIRECT COMPARISON WITH PRIOR STUDIES

1180

1181 We discuss how our approach differs from prior studies, particularly SmoothQuant (Xiao et al., 2023)
 1182 and Harma et al. (2025). Our contribution lies in establishing a general analysis for understanding
 1183 compression order across diverse methods, whereas these prior works either focus on single-method
 1184 optimization or analyze specific method pairs under restrictive assumptions.

1185

1186 **SmoothQuant (Xiao et al., 2023).** SmoothQuant addresses a fundamentally different problem than
 1187 joint compression order optimization. Specifically, SmoothQuant optimizes a *single* compression
 1188 technique (quantization) by mitigating activation outliers through per-channel scaling transformations.
 1189 While the paper states that “SmoothQuant is orthogonal to quantization schemes,” this refers to

1188 its compatibility as a pre-processing step that can be applied before various quantization methods.
 1189 However, SmoothQuant does not examine the order-dependent interaction problem when combining
 1190 quantization with other compression families such as pruning. In contrast, our work focuses on
 1191 understanding how compression order affects model performance when sequentially combining
 1192 methods from different compression families. SmoothQuant may serve as a component within our
 1193 quantization baselines (i.e., as a pre-processing step before quantization), but our analysis operates at
 1194 a higher level—determining the optimal ordering between different model compression techniques
 1195 regardless of the specific quantization implementation. This distinction is critical: SmoothQuant
 1196 addresses *intra-method* optimization (improving quantization itself), while we address *inter-method*
 1197 composition (ordering across different compression types).

1198 **Harma et al. (2025).** As noted in Section 2, only a few studies have addressed how the order of
 1199 compression methods affects model performance. Among them, Harma et al. (2025) stands out as the
 1200 only study that attempts a theoretical approach to the problem. They examine the interaction between
 1201 pruning and quantization, showing that the two are not orthogonal as assumed by previous works.
 1202 Furthermore, they argue that pruning followed by quantization is universally optimal.

1203 However, their framework suffers from three significant limitations. First, their framework relies
 1204 on oversimplified assumptions that hinder practical applicability. Specifically, they focus solely on
 1205 magnitude-based pruning (removes weights based on their absolute values) and max-scaled block-
 1206 wise quantization (uniformly rescaling blocks using their maximum value), both of which are naïve
 1207 approaches that are less practical and often fail to preserve accuracy. Second, their analysis is confined
 1208 to a minimal set of scenarios, failing to address diverse architectures or methods. Beyond the limited
 1209 set of methods, their experiments also consider only the combination of two techniques—pruning
 1210 and quantization—on decoder-based LLMs, lacking broader coverage of models and compression
 1211 approaches. Lastly, the framework cannot be generalized across different settings, as many coun-
 1212 terexamples have shown that pruning-before-quantization is not always optimal. Motivated by these
 1213 gaps, we aim for a more general formulation that holds across methods, models, and metrics, thereby
 1214 introducing the Progressive Intensity Hypothesis.

1215 D.6 VIOLATION CASES OF THE HYPOTHESIS

1216 Although our hypothesis is highly general and robust, we still observe cases where it does not hold.
 1217 These cases largely fall into three categories: severe performance collapse, full model re-training,
 1218 and increase of order-affected layers. First, each model exhibits a different tolerance to compression,
 1219 with performance dropping exponentially beyond a certain ratio. While these settings are impractical
 1220 due to severe performance loss, we observe cases where applying the stronger method first performs
 1221 better. This may be because the error is already too large, violating our assumption of well-designed
 1222 compression in Section 4; applying the stronger method first might help reduce the total error. For
 1223 less compression-robust models like decoder-based LLMs, we observe earlier breakdowns—such as
 1224 diminishing advantage when pruning ratio increases at fixed bit-width (Figure 3a). Second, when
 1225 strong full-training is applied, the advantage from compression order may invert. Compression order
 1226 serves merely as initialization, and the retraining process dominates, making it difficult to attribute
 1227 outcomes to order alone. We plan to investigate these and potentially other exceptions more rigorously
 1228 in future work. Lastly, in practical situations, increasing $C_{\mathcal{P}}$ may result in increase of order-affected
 1229 layers, leading to a violation of the hypothesis. We analyze the details in the following paragraph.

1230 **Impact of $C_{\mathcal{P}}$.** Without loss of generality, we consider only when $C_{\mathcal{P}}$ increases. Increasing $C_{\mathcal{P}}$
 1231 implies a stronger pruning effect, since it lowers $\mathcal{M}(\mathcal{P}(\phi))$, resulting in a decrease in $\mathcal{G}(\mathcal{P}, \mathcal{Q})$ and a
 1232 corresponding increase in $C_{\mathcal{P}}^*$. Hence, to ensure monotonicity and satisfy Hypothesis 1, $\mathcal{A}(\mathcal{Q} \rightarrow \mathcal{P})$
 1233 should increase accordingly. Note that $C_{\mathcal{Q}}$ is fixed while analyzing the effect of $C_{\mathcal{P}}$.

1234 To analyze the effect of increasing $C_{\mathcal{P}}$, we first consider a local step in which the total number of
 1235 pruned units increases by one. For the initial pruning ratio p and the increased ratio p' under the same
 1236 granularity $t_{\mathcal{P}}$, the following relation holds:

$$1238 p' \cdot |\mathbb{U}(\phi; t_{\mathcal{P}})| = p \cdot |\mathbb{U}(\phi; t_{\mathcal{P}})| + 1.$$

1239 From the definition of compression ratio $C_{\mathcal{P}} = 1/(1-p)$, larger pruning ratios correspond to larger
 1240 compression ratios. By repeating this incremental process, we can construct any pruning ratio. Under
 1241 disjoint selectivity, each unit is exclusively assigned to one compression method, allowing us to
 partition the units into four disjoint groups as discussed in Appendix B.1.

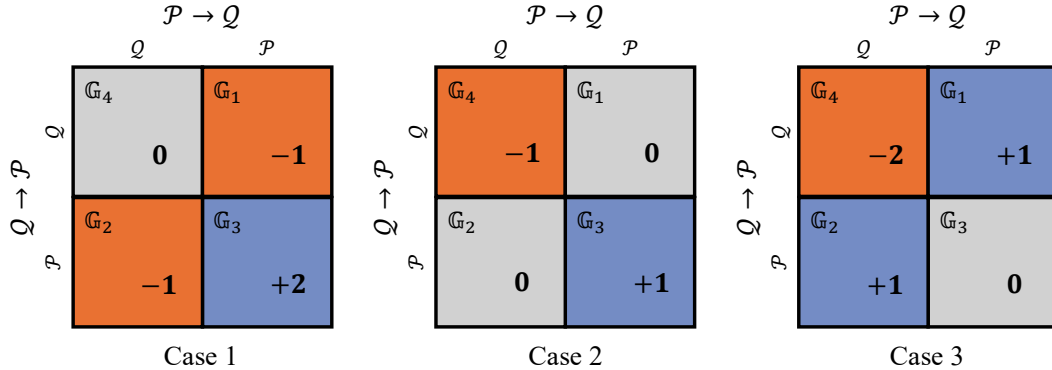


Figure 16: If the number of pruned units increases by one, the change in unit allocation across groups fall into three distinct cases. See Appendix D.6 for details.

Increasing the pruning ratio from p to p' result in three possible changes in the group configuration: the number of affected layers 1) decreases by one, 2) remains unchanged, or 3) increases by one. The three cases are visualized in Figure 16. From Theorem 1, $\mathcal{A}(\mathcal{Q} \rightarrow \mathcal{P}) = \beta \cdot (\sum_{l_i \in \mathbb{G}_2} g(l_i) - \sum_{l_i \in \mathbb{G}_1} g(l_i))$ (where $g(l_i) = \|\delta_{\mathcal{Q}}(\mathbf{W}_i, \mathbf{X}_i)\|_F^2 - \|\mathbf{W}_i \mathbf{X}_i\|_F^2$) should be preserved or increased to satisfy Hypothesis 1. However, this condition is fulfilled in only Cases 1 and 2, but not in Case 3.

- **Case 1: Number of layers affected by order decreases by one.** If a layer is no longer affected by compression due to order change, then another layer must also be excluded to preserve the total number of pruned layers which should be increased by one. Thus, $|\mathbb{G}_1|$ and $|\mathbb{G}_2|$ each decrease by one, while $|\mathbb{G}_3|$ increases by two. Similar to Case 1 of Appendix B.2, as the increase in $C_{\mathcal{P}}$ eliminates a negative loss term, $\mathcal{A}(\mathcal{Q} \rightarrow \mathcal{P})$ increases.
- **Case 2: Number of layers affected by order remains unchanged.** If the additionally pruned layer is always pruned regardless of the compression order, then $|\mathbb{G}_3|$ increases by 1 while $|\mathbb{G}_4|$ decreases by 1. Similar to Case 2 of Appendix B.2, as the loss-contributing groups \mathbb{G}_1 and \mathbb{G}_2 do not change, the compression order advantage $\mathcal{A}(\mathcal{Q} \rightarrow \mathcal{P})$ remains unaffected.
- **Case 3: Number of layers affected by order increases by one.** The aforementioned two cases could not increase the number of order-dependent units, whereas there should exist a case where both groups $|\mathbb{G}_1|$ and $|\mathbb{G}_2|$ increases by one. As the number of total pruned layers should be increased by one, the added layers should be originated from \mathbb{G}_4 , i.e., $|\mathbb{G}_4|$ decreases by two. In contrast to Case 1, $\mathcal{A}(\mathcal{Q} \rightarrow \mathcal{P})$ may decrease due to the increase of negative loss terms.

As the conditions under which each case emerges differ across specific configurations, this phenomenon is not analyzed in general settings. We leave a precise characterization of the conditions under which increasing the pruning ratio may invalidate the progressive intensity hypothesis as an important direction for future work.

D.7 ADDITIONAL REMARKS

Limitations of Current Work. We introduce a broadly applicable hypothesis that can be extended to diverse compression methods and model types across different domains. Still, we acknowledge three important limitations in our current work. First, due to the general nature of our framework, it does not provide detailed analysis for each specific combination of methods. While our hypothesis captures high-level trends, it does not define the best compression sequence for individual cases. This motivates research into discovering the best compression orderings under practical scenarios. Second, our study is limited to joint model compression in plug-and-play settings where methods are combined post-hoc. As demands for higher compression grow, integrated design strategies should be investigated beyond simple combinations. Lastly, our framework does not yet provide explicit predictive rules or precise estimation of how much better one compression order is than another. Capturing the nonlinear and cross-layer effects required for precise sign or value prediction of compression-order advantage $\mathcal{A}(\cdot)$ remains an open problem. We therefore consider the development of predictive models for \mathcal{A} and meta-learning approaches for automatic order selection as a promising direction for future research.

1296 **Future Work.** In addition to addressing the aforementioned limitations, future directions may also
1297 include extensions of our current framework. First, a systematic study of interference across different
1298 pipeline designs would provide deeper insights beyond our current empirical findings. Another
1299 direction is to automate compression order selection based on observed trends. A unified approach
1300 that generalizes across cases may offer a better understanding on the role of compression order. Lastly,
1301 evaluating our hypothesis on emerging architectures such as Mixture-of-Experts and multimodal
1302 LLMs may broaden its generality.

1303 **Usage of AI Assistants.** We employ ChatGPT³ (GPT-4o) and Perplexity⁴ exclusively for language
1304 polishing purposes; for improving grammar and clarity at the sentence level. We do not use them for
1305 any research-related tasks, including code implementation, theoretical derivation, and result analysis.

1306

1307

1308

1309

1310

1311

1312

1313

1314

1315

1316

1317

1318

1319

1320

1321

1322

1323

1324

1325

1326

1327

1328

1329

1330

1331

1332

1333

1334

1335

1336

1337

1338

1339

1340

1341

1342

1343

1344

1345

1346

1347

1348

1349

³<https://chatgpt.com/>

⁴<https://www.perplexity.ai/>